A STRUCTURALLY BASED INVESTIGATION OF ABDOMINAL AORTIC ANEURYSMS IN MOUSE MODELS

A Dissertation

by

MELISSA JILL COLLINS

Submitted to the Office of Graduate Studies of
Texas A&M University
in partial fulfillment of the requirements for the degree of

DOCTOR OF PHILOSOPHY

December 2011

Major Subject: Biomedical Engineering

A Structurally Based Investigation of Abdominal Aortic Aneurysms in Mouse Models

A STRUCTURALLY BASED INVESTIGATION OF ABDOMINAL AORTIC ANEURYSMS IN MOUSE MODELS

A Dissertation

by

MELISSA JILL COLLINS

Submitted to the Office of Graduate Studies of
Texas A&M University
in partial fulfillment of the requirements for the degree of

DOCTOR OF PHILOSOPHY

Approved by:

Chair of Committee,	Mary McDougall
Committee Members,	Alvin Yeh
	Matthew Miller
	Michael Moreno
Head of Department,	Gerard Coté

December 2011

Major Subject: Biomedical Engineering

ABSTRACT

A Structurally Based Investigation of Abdominal Aortic Aneurysms in Mouse Models.

(December 2011)

Melissa Jill Collins, B.S., University of Nebraska - Lincoln

Chair of Advisory Committee: Dr. Mary McDougall

Understanding the mechanical properties of Abdominal Aortic Aneurysms is paramount to improving treatment of this deadly condition. Here, we present work that makes strides in understanding not only the mechanical behavior and constitutive parameters of the two vessels that experience AAAs in different models, but also the effects of three major components of AAA formation. Biaxial mechanical tests were performed using a modified computer-controlled device.

We examined the solid mechanics of the infrarenal and suprarenal aorta to examine why non-targeted models of AAAs (like Ang-II infusion) form exclusively in the suprarenal aorta, whereas in humans the lesions preferentially form in the infrarenal aorta. The major differences between the two vessels are the elastin content and lamellar thickness in the suprarenal aorta.

We analyzed the mechanical and constitutive effects of an acute loss of functional elastin via intraluminal exposure to elastase. We found that, after elastase exposure, vessels were less distensible and experienced non-uniform, but modest

dilatation. The constitutive parameters reflect elastin loss and increased collagen loading.

We detailed the loss of smooth muscle cell contractility as found in human lesions that form in the thoracic aorta. We examined wild-type (WT), heterozygous (HET), and null (KO) α-smooth muscle actin (α-SMA) mice. The data and associated constitutive parameters were nearly identical among the three groups.

We studied the biaxial mechanical tests on Angiotensin-II-infused ApoE-/- mice. This model is a common model of AAA; however, instead of dilation and a thinning of the wall as in AAAs, Ang-II results in a dissecting aneurysm with adventitial growth. The pressure-diameter curves show a lack of sigmoidal shape attributed to elastin; there is some distensibility. The pressure-force behavior of these vessels is similar to a native vessel, unlike the pressure-force behavior of the elastase vessels.

We have added a piece to the puzzle in understanding why AAAs occur preferentially in the suprarenal in mice as opposed to the infrarenal in humans. Our work with the α-SMA mice introduces the idea that missense mutations in the ACTA2 gene, rather than the knocking out of the gene, lead to vascular diseases. We have increased the knowledge of the Ang-II infusion model by presenting biaxial mechanical data of the resulting dilatations. We have also further explored this widely used AAA model via histology to determine that in it is not a model for aneurysm development, but is a dissecting adventitial disease.

DEDICATION

To the mentors and instructors who believed in me and guided me to this day, Dr. David Allen, Dr. David Jones, Dr. Greg Bashford, Dr. Jay Humphrey

In remembrance of Allison Reimer, taken from this life too young by a cerebral aneurysm

"Never doubt that a small group of thoughtful, committed citizens can change the world. Indeed, it is the only thing that ever has."

- Margaret Mead

ACKNOWLEDGEMENTS

This work would not have been possible without the support of many people during my career at Texas A&M. My deepest appreciation goes to my mentor Dr. Jay Humphrey, whose unwavering support, guidance, and belief in this project mean the world to me. To Dr. Mary McDougall, my committee chair for willingly stepping up to the plate when Dr. Humphrey moved to Yale. To my committee Dr. Alvin Yeh, Dr. Michael Moreno, and Dr. Matthew Miller, who offered me their support and guidance. Appreciation is owed to Dr. Emily Wilson, who gave me lab space and a sense of perspective when everything went up in flames.

My colleagues at Texas A&M, whose novel ideas and insights I could not dispense with, Dr. John Eberth and Dr. Hallie Wagner. My fantastic undergraduate workers, without whom this would have been a less interesting and slightly longer road, Jaclyn (Boone) Estes and Matthew Bersi, both are genuinely interested in the future of vascular biomechanics.

Most importantly, is my love for my family. For my parents, who always believed I could do anything I put my mind to, without their support, I could never have done the work involved. My mother, who figures, the "real world" is out there…I just may never find it! My husband, Joe, who helped keep me grounded in reality, and gives me the strength to come back from anything. My daughter, Caitlin, whose laughter reminds me that there is always something to laugh at, if only we could see it from her perspective.

TABLE OF CONTENTS

CHAPTER Page

LIST OF FIGURES

FIGURE Page

FIGURE Page

FIGURE Page

LIST OF TABLES

CHAPTER I

INTRODUCTION: BACKGROUND AND SIGNIFICANCE

Abdominal Aortic Aneurysms (AAAs) are defined as a localized dilatation of the infrarenal aorta greater than 50%; they are responsible for more than 15,000 deaths each year in the United States (the 13th leading cause of death) and are the 10th leading cause of death in men over the age of 55. Approximately 30-50% of patients with a ruptured AAA die before reaching a hospital. Even with surgery there is a 50-70% mortality rate. Since most AAAs are asymptomatic prior to rupture, it is important to understand the mechanics of how they develop so that early detection can lead to earlier interventions.

It is well known that blood vessels adapt to perturbations in chemical and mechanical stimuli over both the short and long term. Changes in mechanical stresses can result from a change in blood pressure, blood flow, or vessel length. When short-term responses, due primarily to changes in smooth muscle cell contractility, are not sufficient to restore stresses toward normal, long-term responses can include cell and matrix turnover that also change the geometry, structure, and mechanical properties of the vessel. Indeed, it appears that changes in contractility and turnover usually work together to restore the vessel toward normal (Valentin et al., 2009). For example, when the blood pressure is chronically elevated (called hypertension), blood vessels

---

This dissertation follows the style of Journal of Biomechanics.

experience an increased wall stress, which often causes a thickening of the wall, but a decreased friction (i.e., wall shear stress) between the flowing blood and the wall, which often causes an increased contraction. In addition, high blood pressure may also increase chemicals within the blood (e.g., angiotensin) that can both increase smooth muscle contraction and promote inflammation in the vascular wall.

There is a pressing need, however, to delineate the separate components of diseases, particularly in the development and progression of diseases such as AAA. The three major components of AAA formation include elastin degradation, smooth muscle actin dysfunction, and inflammation. Here we want to explore the effects of each component on the wall mechanics of the aorta.

The aorta is made up of three layers; the intima, media, and adventitia. The media layer contains smooth muscle cells (SMC) arranged circumferentially, multiple layers of elastin, and collagen types I, III, and IV. The layers of elastin allow the aorta to have a high distension during systole and to recoil during diastole, thus propagating the blood flow and allowing down-stream vessels to experience a nearly steady flow. Elastin fibers in the vasculature are not repaired or regenerated, thus damage to them in permanent.

To study the effects of loss of elastin, we exposed the aorta to porcine pancreatic elastase. Elastase is a protease that, in the presence of calcium, disrupts the elastin fibers. Intraluminal infusion of elastase is frequently used to study aneurysm development (Anidjar et al., 1990; Anidjar et al. 1994; Dobrin and Canfield, 1984; Thompson et al. 2006). When delivered to an artery under pressure, elastase results in

fragmentation of loss of the elastic laminae and the vessel loses its ability to recoil after distension. Although smooth muscle contraction could, theoretically, offset the loss of elastin and help restore the aorta to its original diameter, there tends to be a loss of smooth muscle contractility as well. *In vivo*, these combined effects will lead to a remodeling of the vessel wall (initially a thinning, then a deposition of collagen) that appears to seek to restore to a homeostatic value of circumferential stress. If the damage to the elastic fibers is significant, this response will include a dramatic increase in diameter of the vessel and thinning of the wall. Elastase alone does not cause aneurysms, however. Rather, it is believed that although experimentally delivered elastase is the initial trigger, subsequent inflammatory responses also play roles (Manning et al., 2003; Thompson et al., 2006).

Smooth muscle α-actin is the most abundant protein in adult vascular smooth muscle cells and is necessary for the generation of force in the vasculature. Mutations in the α –SMA encoding gene ACTA2 in humans leads to Thoracic Aorta Aneurysms that lead to Aortic Dissection (TAAD) (Guo et al., 2007). Aortic tissue analyzed from individuals with ACTA2 mutations showed fragmentation and loss of elastin fibers and decreased SMC, indicative of medial degeneration.

In a typical smooth muscle cell, the actin filament interacts with the myosin fibers in the presence of calcium to cause the cell to contract. In vascular smooth muscle cells, the loss of functional α-actin results in decreased contractility of blood vessels (Schildmeyer et al., 2000). In the smooth muscle α-actin knockout mice developed by Dr. Robert Schwartz, Baylor College of Medicine, the loss of actin does not change the

composition of the aorta (smooth muscle cells and elastin are both present), but it does effect the functionality of the blood vessels (Schildmeyer et al., 2000). An ex vivo study of the vascular mechanics of SM α-actin null mice is necessary, however, to quantify the vascular adaptation to the loss of contractility.

Angiotensin-II (Ang-II) is a multifaceted peptide. It serves as a potent vasoconstrictor and plays a role in vascular hypertrophy. Not only does Ang-II act on the vasculature directly, it also does so indirectly. Ang-II also acts on the kidneys, adrenal glands, and the brain. Through various pathways, Ang-II increases blood volume via increased fluid intake and increased renal sodium and fluid retention. Increased blood volume and blood pressure cause vascular remodeling. Ang-I to Ang-II conversion is a primary target for hypertension medications (Klabunde 2005).

Ang-II not only effects blood volume and pressure, it also plays a role in vascular inflammation. Inflammation is generally understood to involve three main steps: increased vascular permeability, increased leukocyte infiltration of the vessel wall, and vessel remodeling. Studies show that Ang-II plays a role in each of these steps (Cheng et al., 2005). Ang-II can increase vascular permeability through damage to the endothelial layer due to pressure changes and via binding to AT_1 receptors. AT_1 receptor binding triggers a host of other effects, including vascular smooth muscle cell proliferation (tissue growth), restriction of blood flow to the renals, and leukocyte infiltration. Leukocyte infiltration is mediated by Ang-II because it not only activates circulating inflammatory cells, it also upregulates pro-inflammatory mediators leading to monocyte adhesion to the endothelial cells (Cheng et al., 2005).

Unlike the elastase model, which is designed to target the infrarenal aorta, the Ang-II model is a systemic model; it is typically delivered sub-cutaneously. In this model, aneurysms form in the suprarenal aorta as opposed to the infrarenal aorta. In humans, AAAs occur strictly in the infrarenal portion of the aorta. Thus it is necessary to look at the mechanical differences between the infrarenal and the suprarenal aorta in order to better understand the site preference in different species.

Stress is an important measure in vascular biomechanics since it is a key mediator in growth and remodeling (Baek et al., 2006; Humphrey and Rajagopal 2003). Since aneurysms are, by definition, thin-walled, the 2D assumption is especially appropriate, thus the radial component of stress is ignored. The circumferential ($\sigma_{\theta\theta}$) and axial (σ_{zz}) stresses are defined (Gleason and Humphrey, 2005; Humphrey 2002):

$$\sigma_{\theta\theta} = \frac{Pr_i}{r_a - r_i} \qquad \sigma_{zz} = \frac{f_T + \pi r_i^2 P}{\pi h(2r_i + h)} \tag{1.1-1.2}$$

where P is the transmural pressure, f is the axial force on the vessel as defined by $f = f_T + \pi r_i^2 P$, with f_T being the force measured by the force transducer, and r_a and r_i being the outer (adventital) and inner (intimal) radius of the loaded vessel. Stretch calculations are based on the unloaded configuration, thus using mid-wall radius values ($r_{mid} = (r_a - r_i)/2$).

$$\lambda_\theta = \frac{r_{mid}}{R_{mid}} \qquad \lambda_z = \frac{l}{L} \tag{1.3-1.4}$$

where R_{mid} and L are the unloaded mid-wall radius and unloaded length respectively and l is the current length.

A theoretical framework has been established for modeling wall stress. The model makes the following assumptions: vessel behavior is nonlinear, anisotropic, isothermal, and incompressible. The Cauchy stress is (Humphrey, 2002):

$$t = 2F\frac{\partial W}{\partial C}F^T - pI \tag{1.5}$$

where C is the left Cauchy-Green tensor ($C=F^TF$, F is the deformation gradient tensor) and W is the strain energy function. Holzapfel et al.(2000, 2004) proposed a strain energy function that accounts for the neo-Hookean (isotropic) and anisotropic contributions of wall constituents (elastin and collagen). This function was later adapted to a four-fiber family model by Baek et al. (2007). When considering the aorta to be a homogenized layer, the strain energy function is:

$$W = \frac{c}{2}(I_c - 3) + \sum_{k=1-4}\frac{c_1^k}{4c_2^k}\{exp[c_2^k((\lambda^k)^2 - 1)^2] - 1\} \tag{1.6}$$

$$I_c = \lambda_r^2 + \lambda_\theta^2 + \lambda_z^2 \tag{1.7}$$

$$\lambda^k = \sqrt{\lambda_\theta^2 sin^2\alpha^k + \lambda_z^2 cos^2\alpha^k} \tag{1.8}$$

$$\{\alpha^1 = 0, \alpha^3 = -\alpha^2, \alpha^4 = \pi/2\} \tag{1.9}$$

where α^k is the angle of the k^{th} fiber family with respect to the axial direction (see Figure 1.1) and the constants c, c_1^k, and c_2^k are material parameters found via nonlinear regression.

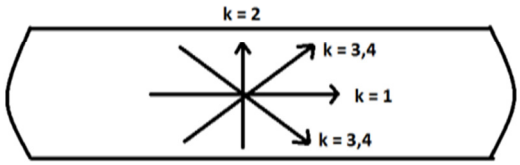

Figure 1.1. Schema of the directions of the four fiber families in the proposed constitutive models. Collagen fiber directions for k = 1-4.

We have applied these fundamental mechanics to the components of AAA formation. Specifically, we have looked at each component individually, which has not been done previously. Specifically, we compared the mechanics of the infrarenal and the suprarenal aorta; we evaluated the effects of an acute loss of functional elastin in the aorta; studied *in vivo* effects on the biaxial mechanics of the smooth muscle α-actin knockout mouse and attempted to characterize the mechanical behavior of lesions that occurred in Ang-II infused mice.

CHAPTER II

MECHANICAL PROPERTIES OF SUPRARENAL AND INFRARENAL ABDOMINAL AORTA: IMPLICATIONS FOR MOUSE MODELS OF ANEURYSMS[1]

Overview

Multiple mouse models have been developed to increase our understanding of the natural history of abdominal aortic aneurysms. An advantage of such models is that one can quantify the time course of changes in geometry, histology, cell biology, and mechanics as a lesion develops. One of the most commonly used mouse models yields lesions in the suprarenal abdominal aorta whereas most other models target the infrarenal abdominal aorta, consistent with the clinical observation that nearly all abdominal aneurysms in humans occur in the infrarenal aorta. Understanding reasons for similarities and differences between diverse mouse models and human lesions may provide increased insight that would not be possible studying a single situation alone. Toward this end, however, we must first compare directly the native structure and properties of these two portions of the abdominal aorta in the mouse. In this paper, we present the first biaxial mechanical data and nonlinear constitutive descriptors for the suprarenal and infrarenal aorta in mice, which reveals only subtle mechanical differences

[1] Reprinted with permission from Mechanical Properties of Suprarenal and Infrarenal Abdominal Aorta: Implications for Mouse Models of Aneursysms by Collins, M.J., Bersi, M., Wilson, E., Humphrey, J.D. 2011. *Medical Engineering and Physics,* Copyright [2011] by Elsevier.

despite marked morphological and histological differences. Such data promise to increase our ability to understand and model the natural history of these deadly lesions.

Introduction

Abdominal aortic aneurysms (AAAs) are currently the 13th leading cause of death in the United States. These lesions typically present in older patients and thus are expected to become increasingly problematic in our aging society. AAAs are characterized by a loss or fragmentation of intramural elastin, apoptosis of smooth muscle cells, inflammation, and remodeled collagen, which together allow a localized dilatation of the wall; in most cases, AAAs also associate with atherosclerotic development and the enlarged lumen is the site of intramural thrombus. Despite significant advances in our understanding of both the biomechanics (Duo and Dalman, 2010; Vorp, 2007) and the pathophysiology (Shimizu et al., 2006; Thompson et al., 2006), much remains unknown regarding the natural history of these deadly lesions. In particular, our lack of understanding stems largely from the difficulty of obtaining longitudinal information from patients. There is, therefore, a pressing need for more data on the evolving geometry, histology, hemodynamics, and mechanical properties as well as the underlying cellular processes that govern these changes. For this reason, mouse models are increasingly used to study the natural history of AAAs.

Three different mouse models have found increased utility in studying the evolution of AAAs. Because of the importance of the loss of elastin, one model relies on the localized removal of intramural elastin via a short term infusion of elastase within the lumen of the infrarenal aorta (Ailawadi et al., 2009; Goergen et al., 2011). This acute

loss of elastin allows the wall to dilate slightly, but it also incites a subsequent inflammatory process that leads to the development of an AAA (usually defined by a 1.5 or more fold increase in diameter). Because of the common association of atherosclerosis with AAAs, another model is based on the application of calcium chloride to the adventitial surface of the infrarenal aorta, which initiates an inflammatory process involving atherosclerotic characteristics and results in the development of a dilated wall (Sheth et al., 2010). Finally, motivated by roles of atherosclerosis, hypertension, and inflammation in the development of AAAs, another model uses a long-term subcutaneous infusion of angiotensin-II (Ang-II), often in the apolipoprotein-E null (ApoE-/-) mouse (Cassis et al., 2009; Deguchi et al. 2009). Although Ang-II increases blood pressure, it primarily incites an inflammatory response that often leads to AAAs. Interestingly, however, these Ang-II infusion models yield AAAs in the suprarenal rather than the infrarenal aorta, and dissection often precedes dilatation (Saraff et al., 2003). It appears that this site arises in part from the propensity of atherosclerotic lesions to develop in the suprarenal rather than infrarenal aorta in ApoE-/- mice (Hayenga et al., 2011; Nakashima et al. 1994), but also the different hemodynamics (Amirbekian et al., 2009) and possibly wall properties in the suprarenal aorta. For a more extensive review of mouse models of AAAs, see Daughtery and Cassis (2004).

A complete understanding of processes that lead to the initiation and enlargement of an AAA must include knowledge of the mechanics of the arterial wall from which the lesion arises. In the case of current mouse models of AAAs, there is thus a need to

understand the possibly different mechanics of the suprarenal and the infrarenal abdominal aorta. Indeed, understanding reasons for the differential development of lesions in different mouse models and humans may provide insight not possible by analyzing a single situation. In this paper, we present the first direct comparison of the biaxial mechanical behaviors of these two types of vessels in the mouse and quantify the data using a nonlinear constitutive relation that was recently shown to be useful in describing the mechanical behavior of both aging human abdominal aorta and abdominal aortic aneurysms (Ferruzzi et al., 2011).

Methods

Specimen Preparation. All animal protocols were approved by the Texas A&M University Institutional Animal Care and Use Committee and followed methods used previously in our laboratory (Dye et al., 2007; Eberth et al., 2009b). Briefly, following an overdose of sodium pentobarbital, the abdominal aorta was harvested by gentle dissection from 8 to 12 week old male mice using a dissection microscope. The suprarenal aorta was excised from the diaphragm to between the left and right renal arteries; the infrarenal aorta was similarly excised from between the left and right renal arteries to immediately proximal to the aortic trifurcation. All vessels were trimmed of excess adventitial tissue, cannulated using custom drawn glass pipettes, and secured to the cannulae using 6-O suture. Branches were ligated with suture to enable the specimen to be pressurized when mounted in a modified version of our computer-controlled biaxial testing device (Gleason et al., 2004). The testing chamber was filled with a standard phosphate buffered saline solution and maintained at 37°C.

Testing Protocols. The original unloaded outer diameter and axial length of the mounted specimen (i.e., at zero pressure and zero axial force) were measured interactively using a video-microscope and custom LabView software, with each measurement repeated for verification. Following a subsequent acclimation period of 15 minutes at a luminal pressure of 80 mmHg and an axial stretch of 1.5 (i.e., at the mean *in vivo* stretch determined in pilot studies), the artery was preconditioned at this stretch via 3 cycles of pressurization from 10 to 140 mmHg at ~2 mmHg/sec. This loading rate is consistent with that used in most studies of arterial mechanics and is motivated by the relative strain-rate insensitivity exhibited by most arteries (Humphrey 2002). The nearly unloaded outer diameter and axial length were measured again, this time at a pressure of 5 mmHg to prevent the vessel from collapsing; there were typically minimal increases in dimensions relative to measurements taken prior to acclimation and preconditioning. Biaxial data were then collected during cyclic pressurization tests from 10 to 140 mmHg at the same rate and mean *in vivo* stretch as well as at ~5% above and below this stretch. Finally, biaxial data were collected during cyclic extension tests at different constant pressures of 60, 100, and 140 mmHg. These tests were performed such that the axial force ranged from 0 to 24.5 mN for the suprarenal aorta and from 0 to 6 mN for the infrarenal aorta. These values were selected based on findings during pilot tests, which accounted for the much larger cross-sectional area of the suprarenal aorta. Luminal pressure, axial force, outer diameter, and overall axial length were measured on-line using a custom LabView program and recorded continually during testing. Finally, note that the unloaded inner diameter, and thus thickness, was measured using a calibrated

dissection microscope to image intact rings cut from each end of the specimen prior to cannulation; 2 to 3 measurements around the circumference of each ring were averaged to yield mean values for each specimen.

Data Analysis. The biaxial data were converted to mean circumferential and axial Cauchy stresses using standard formulae (Humphrey 2002)

$$t_{\theta\theta}^{\exp} = \frac{P^{\exp} a}{h}, \quad t_{zz}^{\exp} = \frac{f^{\exp}}{\pi h(2a+h)}, \tag{2.1}$$

where a is the inner radius in any loaded state and h is the associated thickness of the wall. The axial force applied to the artery is given by $f^{\exp} = f_T^{\exp} + \pi a^2 P^{exp}$, where $f_T^{\exp}$ is measured by the force transducer and $P^{\exp}$ is measured by the pressure transducer.

We employed a "four fiber family" hyperelastic constitutive model (Ferruzzi et al., 2011) to quantify the measured passive biaxial mechanical behaviors. This model has proven useful in capturing biaxial mechanical responses of diverse mouse carotid arteries (Eberth et al, 2009b; Gleason et al., 2008; Wan et al., 2010). The specific form of the strain energy function is

$$W\left(\mathbf{C},\mathbf{M}^i\right) = \frac{c}{2}\left(I_C - 3\right) + \sum_{i=1}^{4} \frac{c_1^i}{4c_2^i}\left\{ \exp\left[c_2^i \left(I_4^i - 1 \right)^2 \right] - 1 \right\}, \tag{2.2}$$

where c, c_1^i are material parameters having units of stress and c_2^i are dimensionless, $I_C = tr\mathbf{C}$ is the first invariant of the right Cauchy-Green tensor, and $I_4^i = \mathbf{M}^i \cdot \mathbf{C}\mathbf{M}^i$ is the square of the stretch of the i-th collagen fiber family (i.e., $(\lambda^i)^2$). Fiber orientations are defined in the reference configuration by unit vectors $\mathbf{M}^i$, which depend on angles α_o^i defined between fiber and axial directions. Axial and circumferential fibers were

thus defined at $\alpha_o^1 = 0$ and $\alpha_o^2 = 90$ degrees, respectively, while symmetrically oriented diagonal fibers were accounted for via a single parameter, $\alpha_o^3 = -\alpha_o^4 = \alpha_o$. Note that

$$I_4^d = (\lambda^{i=3,4})^2 = \lambda_z^2 \cos^2 \alpha_o + \lambda_\vartheta^2 \sin^2 \alpha_o \,, \tag{2.3}$$

where the superscript *d* denotes "diagonal." These two families of collagen are typically regarded as mechanically equivalent, hence $c_1^3 = c_1^4 \equiv c_1^{3,4}$, $c_2^3 = c_2^4 \equiv c_2^{3,4}$. This overall model thus requires estimation of eight unknown parameters $(c, c_1^1, c_2^1, c_1^2, c_2^2, c_1^{3,4}, c_2^{3,4}, \alpha_o)$ that describe the passive mechanical behavior. Pilot studies suggested that there was little active response in the phosphate buffered saline, hence we used a passive constitutive model alone.

Assuming a 2-D state of stress within the central region of thin-walled biaxially tested arteries, the deformation gradient tensor has the form $\mathbf{F} = \mathrm{diag}\left(\lambda_r, \lambda_\theta, \lambda_z\right)$. Circumferential and axial stretch ratios during finite inflation and extension testing were calculated via

$$\lambda_\theta = \frac{r_{mid}}{R_{mid}}, \quad \lambda_z = \frac{l}{L}, \tag{2.4}$$

where $r_{mid} = (a+b)/2$ and $R_{mid} = (A+B)/2$ represent loaded and unloaded mid-wall radii and, similarly, *l* and *L* represent loaded and unloaded axial length; here *a* and *b* denote loaded inner and outer radii whereas *A* and *B* denote associated unloaded radii. Assuming incompressibility during transient loading, the inner deformed radius was computed from experimentally measurable quantities via $a = \sqrt{b^2 - \bar{V}/\pi l}$, where $\bar{V}$

denotes mean wall volume with $V=\pi(B^2-A^2)L$. Incompressibility also requires that $\lambda_r=1/(\lambda_z\lambda_\theta)$.

For a plane state of stress ($t_{rr}=0$), equation (2.2) yields theoretically calculated Cauchy stresses of the form

$$t_{\theta\theta}^{th}=c\left(\lambda_\theta^2-\frac{1}{\lambda_\theta^2\lambda_z^2}\right)+c_1^2\left(\lambda_\theta^2-1\right)\exp\left[c_2^2\left(\lambda_\theta^2-1\right)^2\right]\lambda_\theta^2+2c_1^{3,4}\left(I_4^d-1\right)\exp\left[c_2^{3,4}\left(I_4^d-1\right)^2\right]\lambda_\theta^2\sin^2\alpha_o,$$
$$t_{zz}^{th}=c\left(\lambda_z^2-\frac{1}{\lambda_\theta^2\lambda_z^2}\right)+c_1^1\left(\lambda_z^2-1\right)\exp\left[c_2^1\left(\lambda_z^2-1\right)^2\right]\lambda_z^2+2c_1^{3,4}\left(I_4^d-1\right)\exp\left[c_2^{3,4}\left(I_4^d-1\right)^2\right]\lambda_z^2\cos^2\alpha_o. \tag{2.5}$$

Best-fit values of the unknown parameters in equation (2.2) were determined using a nonlinear least squares minimization of the error *e* between normalized theoretically predicted (*th*) and experimentally inferred (*exp*) applied loads, namely

$$e=\sum_{i=1}^{N}\left[\left(\frac{P^{th}-P^{\exp}}{P^{avg}}\right)_i^2+\left(\frac{f^{th}-f^{\exp}}{f^{avg}}\right)_i^2\right], \tag{2.6}$$

where *N* is the total number of data points (i.e., equilibrium configurations) for all experimental protocols combined for each specimen and *avg* denotes the overall average value. The error *e* was minimized using the built-in function *lsqnonlin* in MATLAB, subject to physical constraints that $c,\ c_1^i,\ c_2^i\geq 0$ and $0\leq\alpha_o\leq\pi/2$ due to the symmetry of the diagonal fibers.

Histology. At the completion of mechanical testing, all vessels were fixed in 4% formalin in an unloaded state for 1 hour, immersed in a cryoprotectant (30% sucrose) overnight, and placed in optimum cutting temperature medium in 2-methylbutane cooled with liquid nitrogen and stored at -80°C. Frozen samples were sectioned at 5 microns

and stained with either Verhoeff van Gieson (VVG) to identify elastin or hematoxylin and eosin (H&E) to identify cell nuclei and overall morphology. Elastin area fractions were determined using a method of thresholding described previously[17] and were based on one cross-section per sample.

Statistics. Statistical significance was evaluated using either an unpaired Student's t-test or an Analysis of Variance (with $n = 6$ for suprarenal and $n = 6$ for infrarenal specimens taken from separate animals), with significance taken at a level $p < 0.05$.

Results

Biaxial data (i.e., pressure – diameter and axial force – pressure responses at multiple fixed axial stretches) revealed slightly different characteristic behaviors for the suprarenal and the infrarenal aorta (Figures 2.1 and 2.2, respectively). For increased clarity, a reduced number of data (symbols) are shown in these figures; note, too, that the theoretical fits to data achieved using equations 2.1, 2.5, and 2.6 are also shown (solid curves), with associated best-fit values of the model parameters listed in Table 2.1 for all 12 specimens. Two conspicuous differences in behavior are the more sigmoidal pressure – diameter response exhibited by the suprarenal aorta and the larger value of axial force needed to extend the suprarenal aorta over comparable axial stretches. The former is sometimes ascribed to a higher elastin-to-collagen ratio; the latter appeared to be due simply to the greater cross-sectional area of the suprarenal aorta (which can be computed via $\pi h(2a+h)$). The best-fit value of the parameter c, which is thought to model the elastin-dominated portion of the wall (Ferruzzi et al., 2011), was statistically higher for

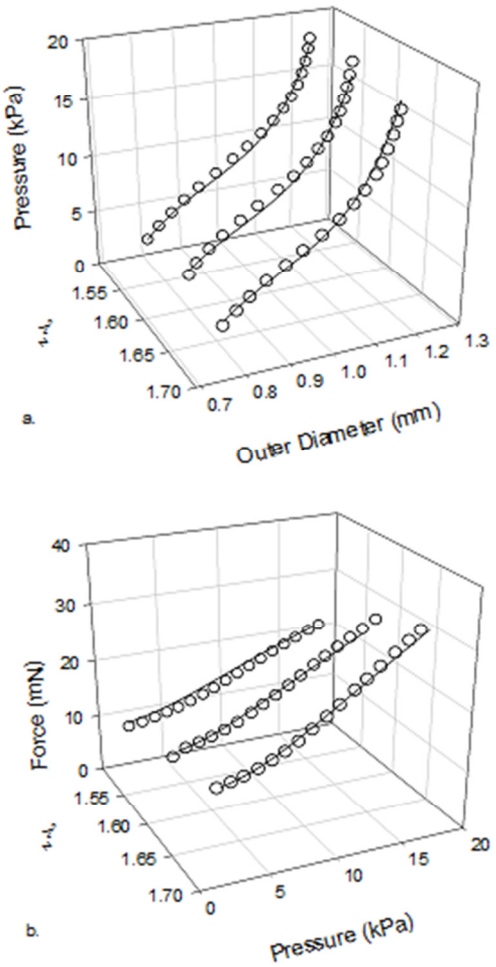

Figure 2.1. Results from pressure – diameter tests at three different fixed axial stretches for the suprarenal. A reduced number of data points (symbols) are shown for clarity; also shown are the fits to data (solid lines) using equation 2.5.

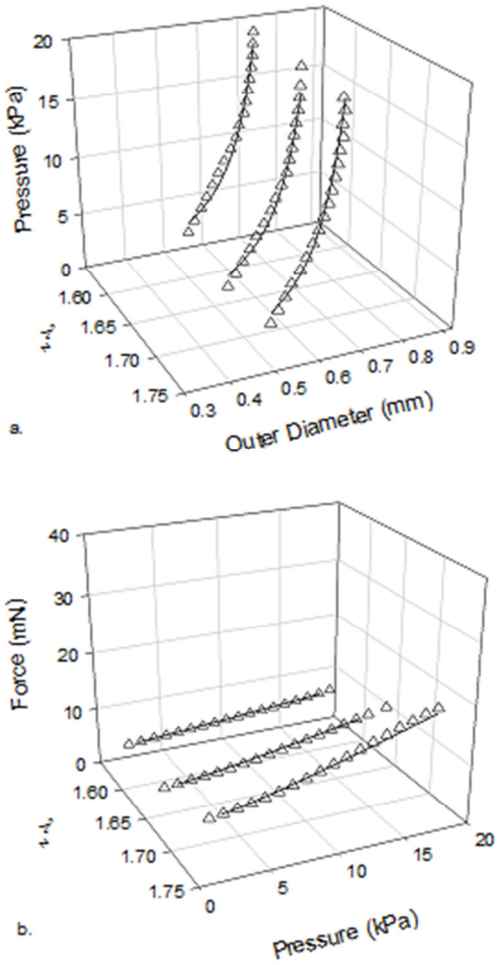

Figure 2.2. Results from pressure – diameter tests at three different fixed axial stretches for the infrarenal abdominal aorta. A reduced number of data points (symbols) are shown for clarity; also shown are the fits to data (solid lines) using equation 2.5.

Table 2.1. Best-fit values of model parameters (equation 2.2) for all 6 suprarenal and 6 infrarenal aorta specimens.

		AXIAL		CIRCUMFERENTIAL		DIAGONAL		
Vessel #	**c (kPa)**	**c_1 (kPa)**	**c_2**	**c_1 (kPa)**	**c_2**	**c_1 (kPa)**	**c_2**	**angle**
SUPRA								
1	15.13	3.13	0.11	7.61	2.84E-09	3.15	0.81	49.20
2	4.07E-10	9.09	1.12E-09	5.51	0.23	8.61	0.46	40.83
3	16.09	14.20	0.01	9.81	0.17	1.07	1.13	34.74
4	30.11	2.51	0.43	4.22	1.38	0.94	2.09	37.69
5	17.51	14.06	0.08	4.55	0.26	1.36	1.49	35.73
6	14.31	15.63	0.01	4.41	0.20	0.57	1.30	31.14
INFRA								
1	5.04	4.82	0.12	6.73	0.06	1.42	0.73	39.59
2	5.57	3.21	0.19	4.97	0.39	0.57	1.43	40.58
3	5.07	7.95	0.00	0.97	0.29	1.11	0.86	36.53
4	3.40	1.41	0.82	2.24	0.28	2.27	0.85	36.87
5	8.26	11.65	0.07	8.24	0.59	0.74	2.69	38.86
6	7.67	8.23	0.44	5.49	0.29	1.23	2.12	35.44
Supra Mean	15.53 ± 9.59	9.77 ± 8.82	0.11 ± 0.16	6.02 ± 2.24	0.37 ± 0.50	2.62 ± 3.07	1.21 ± 0.56	38.22 ± 6.26
Infra Mean	5.84 ± 1.82	6.21 ± 3.76	0.27 ± 0.31	4.77 ± 2.73	0.32 ± 0.17	1.22 ± 0.60	1.45 ± 0.80	37.98 ± 1.99

the suprarenal than the infrarenal aorta (15.53 versus 5.84 kPa, respectively; Table 2.1), also consistent with a greater contribution of elastin to the overall behavior. Indeed, VVG images (Figure 2.3, left) suggested that the suprarenal aorta tended to have an additional musculo-elastic fascicle (i.e., layer of smooth muscle bounded by elastic lamellae), though not in all cases. Moreover, the elastic lamellae appeared to be thicker in the suprarenal aorta. Hence, although wall thickness at *in vivo* conditions differed by only 15% (43.7 and 37.9 microns, respectively; Table 2.2), the percentage of the wall occupied by elastin was 36% higher in the suprarenal aorta (38 and 28%, respectively, which was statistically different based on VVG images). The deformed luminal radius

was also significantly larger in the suprarenal aorta than in the infrarenal aorta, as, for example, a = 488 microns versus a = 305 microns at a common pressure of 80 mmHg and the individual *in vivo* axial stretches. Interestingly, despite differences in cross-sectional area and percent elastin, the *in vivo* stretches (Figure 2.4) were remarkably similar for the two types of vessels: mean values were 1.50 and 1.49 for suprarenal and infrarenal aorta, respectively (Figure 2.4 and Table 2.2), which were not statistically different. Other information, such as animal age and weight and unloaded geometry, is also listed in Table 2.2.

When the biaxial data were plotted as Cauchy stress – stretch, the behaviors of both portions of the abdominal aorta appeared to be characteristically nonlinear, perhaps exponential (Figure 2.5). In these plots, the symbols again represent culled data, but the solid curves now represent predictions rather than fits because pressure / force data were used in the nonlinear regressions. Indeed, with the exception of the parameter c, the best-fit parameters were comparable for the two types of vessels as well (Table 2.1). Because it is difficult to compare overall behaviors based on values of multiple parameters in a nonlinear model, consider the strain energy predicted to be stored, per unit reference volume, at the same levels of pressure (from 60 to 120 mmHg) and the individual *in vivo* axial stretch (Figure 2.6a). As it can be seen, the overall stiffness of the suprarenal aorta tended to be higher than that of the infrarenal aorta, especially at higher pressures. This conclusion was supported by a direct comparison of circumferential stress – stretch behaviors at the *in vivo* stretch (Figure 2.6b). The differences at all pressures from 60-120 mmHg were statistically significant, at a $p < 0.05$ (ANOVA).

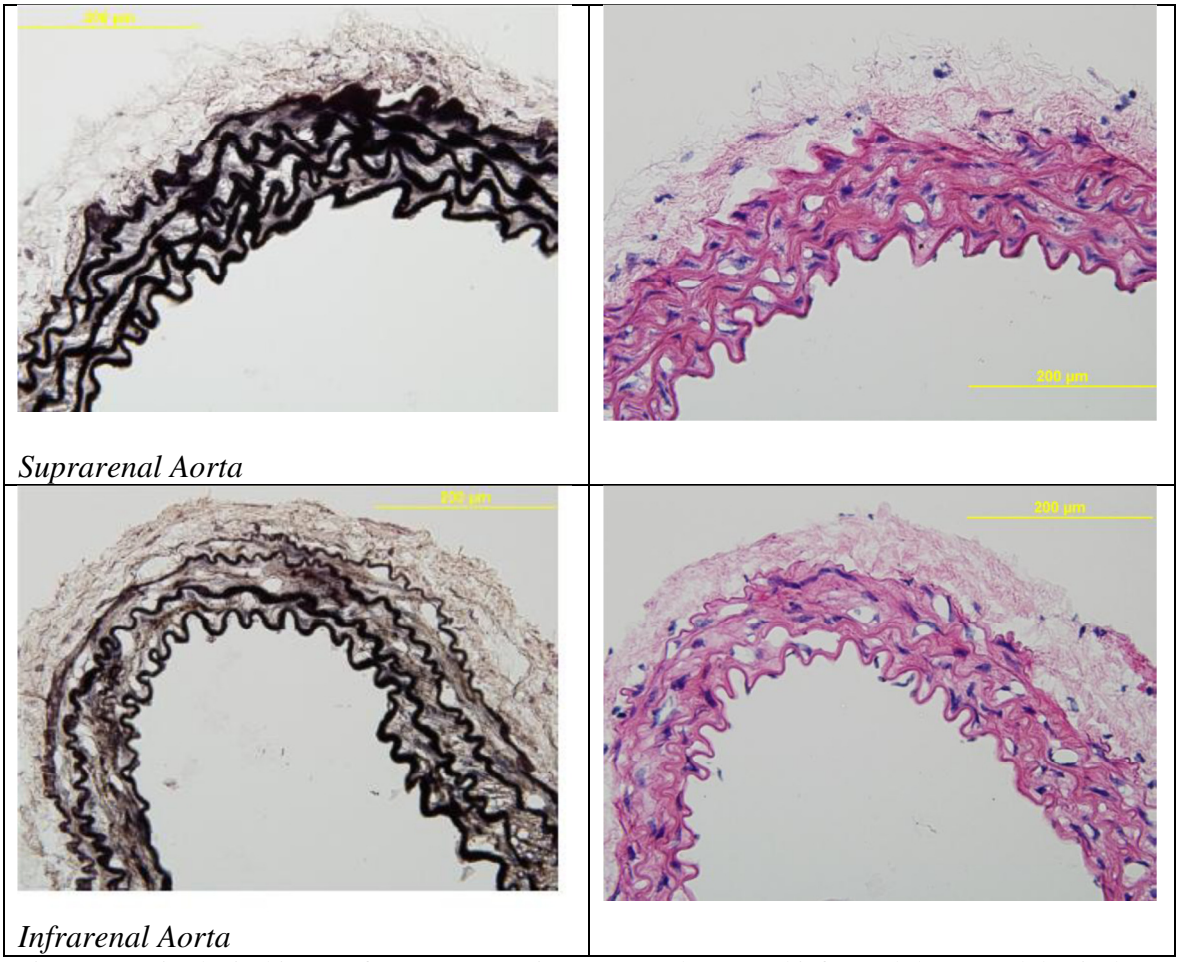

Figure 2.3. Histological images from representative suprarenal (top) and infrarenal (bottom) abdominal aorta from the mouse. Specimens strained with VVG (which reveals elastin as black) are shown on the left and those stained with H&E (which reveals cell nuclei in blue and overall tissue morphology in pink) are shown on the right.

Table 2.2. Mean values of relevant data on age, weight, and geometry of the suprarenal and infrarenal aorta. Note that the length, outer diameter, and thickness are given in the unloaded configuration.

Vessel	**Age** (wks)	**Weight** (g)	**lambda** (--)	$\mathbf{l_o}$ (mm)	$\mathbf{OD_o}$ (um)	$\mathbf{H_o}$ (um)	**a** (um) @80 mmHg	**h** (um) @80 mmHg
Supra	8.9 ± 0.9	22.4 ± 1.9	1.51 ± 0.10	4.50 ± 0.80	787 ± 43	99.1 ± 17.2	488 ± 21	43.7 ± 3.6
Infra	9.7 ± 0.8	21.8 ± 2.5	1.49 ± 0.16	3.35 ± 0.65	523 ± 46	88.8 ± 9.7	303 ± 29	40.0 ± 7.0

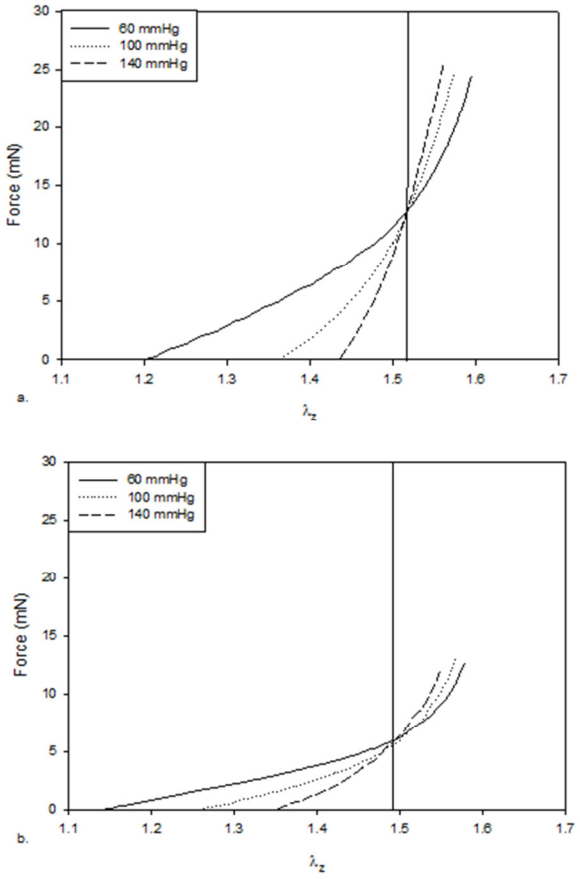

Figure 2.4. Results from axial force – extension tests at three different fixed luminal pressures for the suprarenal (top) and infrarenal (bottom) aorta. The "cross-over" points (vertical lines) estimate the *in vivo* axial stretch, mean values of which were 1.51 and 1.49 for the suprarenal and infrarenal aorta, respectively.

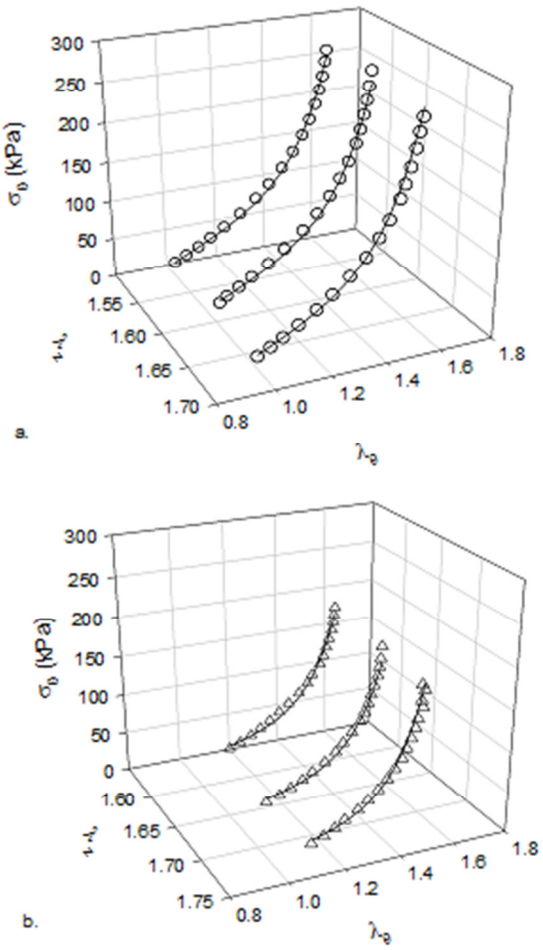

Figure 2.5. Experimentally inferred (symbols) and theoretically predicted (solid curves) circumferential Cauchy stress – stretch responses for the suprarenal (top) and infrarenal (bottom) aorta during cyclic pressurization tests at three different fixed axial stretches.

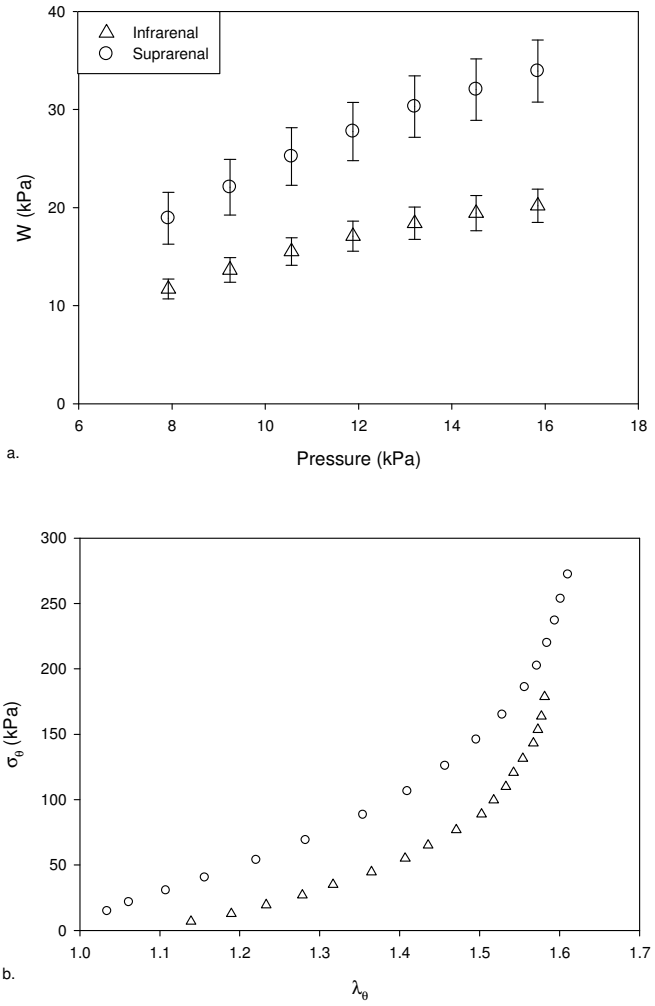

Figure 2.6. Mean values of (top) the computed strain energy stored in the suprarenal (circles) and infrarenal (triangles) at different values of luminal pressure and the individual *in vivo* axial stretch. Note, all pressures have statistical ($p< 0.05$) difference in stored energy. Also shown are mean predicted Cauchy stress – stretch (bottom) responses at the *in vivo* stretch for both the suprarenal (circles) and the infrarenal (triangles) aorta.

Discussion

Aneurysms arise in the human abdominal aorta due to dramatic localized changes in the microstructure of the wall, which in turn alter biomechanical properties significantly (Ferruzzi et al., 2011; Humphrey and Taylor, 2008; Vorp, 2007). Despite

the plethora of papers investigating the biology, and implicating the mechanics, of AAAs in the mouse (Ailawadi et al., 2009; Cassis et al., 2009; Daugherty and Cassis, 2004; Deguchi et al., 2009; Goergen et al., 2011; Saraff et al., 2003; Sheth et al., 2010), there has been almost no attention heretofore to the biaxial mechanical properties of the aortic wall, including possible differences between the suprarenal and infrarenal abdominal aorta that may help explain the different types of aneurysms that occur in common mouse models.

Amirbekian et al.(2009) reported an important comparison of hemodynamic conditions in the mouse suprarenal and infrarenal aorta, the latter of which was contrasted qualitatively to conditions in the human. Despite similar mean blood velocities in the suprarenal and infrarenal aortas, both the mean (15.3 versus 7.5 ml/min) and the maximum (49.3 versus 21.6 ml/min) volumetric flowrate was much lower in the latter because of the high flow to the kidneys. More importantly, however, they found that the infrarenal aorta in the mouse does not experience the flow reversal that is seen in the human infrarenal aorta, which in turn is thought to yield oscillatory shear stresses that may contribute to the development of aneurysms. Given that the suprarenal aorta in the mouse similarly did not experience flow reversal, it was suggested that further studies were needed to determine its susceptibility to aneurysms in the Ang-II infusion model, including fluid-solid interaction (FSI) computations. Such studies obviously require detailed information on multiaxial wall properties, which the present paper provides for the first time. In contrast, with regard to wall properties, Amirbekian and colleagues (2009) merely compared percent distensibility over the cardiac cycle in these

two segments of the aorta (72 ± 26% and 63 ± 18% in the suprarenal and infrarenal aorta, respectively, which were not significantly different). Goergen et al. (2011) similarly reported maximum cyclic Green strains during the cardiac cycle of 20.8 ± 4.2% and 19.4 ± 2.5% in the mouse suprarenal and infrarenal aorta, respectively. Together, these reports suggest that suprarenal and infrarenal aortas have a similar structural stiffness in the mouse, which was suggested to be significantly less than that in the human (Amirbekian et al., 2009).

In vivo structural stiffness depends on the material stiffness, thickness of the wall, axial prestretch, and perivascular support. Of these, only perivascular support was not measured herein. As revealed by Figure 2.4, the axial prestretch was similar in the suprarenal and infrarenal aorta (about 1.5). This finding is similar to the report by Guo and Kassab (2003) that the proximal and distal abdominal aorta have similar axial prestretches (~1.6). These investigators also reported that the circumferential "modulus" was similar at these two sites, but the numerical values must be viewed cautiously because the data were inappropriately reduced assuming linear elastic behavior. Our findings are nonetheless similar, in that the suprarenal aorta tended to be slightly stiffer overall, but not significantly so. Wagenseil et al.(2005) also reported axial prestretches and biaxial stress-stretch data for the abdominal aorta from the mouse, but they did not document which portion of the aorta was used in their study. Their reported value for axial prestretch was also ~1.6. Whereas our value was inferred from cross-over points in axial force – extension tests at multiple pressures (Figure 2.4), both Guo and Kassab and Wagenseil and colleagues measured this value based on the degree of retraction at

excision. Given that the cross-over point is generally regarded as a useful estimate of *in vivo* stretch (Humphrey et al., 2009), it is not clear whether our results near 1.5 differ from these two reports because of our different experimental approach, the gentle removal of loose perivascular tissue prior to our *in vitro* testing, the anesthetics used, the different strains of mice, or so forth. Nevertheless, it is clear that the *in vivo* axial prestretch does not differ significantly from the suprarenal to the infrarenal aorta. Wagenseil and colleagues did not attempt to quantify the measured aortic mechanical behavior, hence it is not possible to compare results directly. Their circumferential Cauchy stress – stretch plots appear to be comparable to the present results, however, with stresses on the order of 200 kPa at circumferential stretches about 1.6 (cf. Figure 2.6).

Data that compare the suprarenal and infrarenal abdominal aorta histologically also appear to be scant. A notable example is the work by Bunce (1974), who compared most large arteries in the dog. Notwithstanding expected differences in the number of musculo-elastic fascicles in the thicker walled dog aorta, a conspicuous difference between the abdominal aorta in the mouse and the dog is the more regular musculo-elastic fascicles in the mouse. That is, the infrarenal aorta, and to a lesser extent the suprarenal aorta, in the dog has a greater density of elastin in the outer one-third of the media, similar to that seen in the dog left common carotid artery. This single example of species-to-species differences reminds us of the need for caution in extrapolating results from mice to men, though a detailed understanding of the reasons for such differences may provide yet increased insight that can be helpful in understanding the human

condition. As seen in Figure 2.3, VVG staining suggested that the suprarenal mouse aorta typically had ~4 musculo-elastic fascicles whereas the infrarenal aorta typically had ~3 fascicles. These findings are consistent with the report by Goergen et al.(2010), who also noted that the suprarenal aorta contains about 50% more elastin than does the infrarenal aorta. Our data (38% versus 28%, or 36% different) are comparable with their findings. Indeed, the higher best-fit value of the model parameter *c* (Table 2.1) is similarly consistent with this finding.

In summary, the present study quantified, for the first time, the mean biaxial mechanical behavior of the suprarenal and infrarenal abdominal aorta in young mature male mice. The same constitutive relation that has proven useful in describing the behavior of the human infrarenal abdominal aorta and human AAAs was found to fit data from mice as well (cf. Figures 2.1 and 2.2). Indeed, even most of the best-fit parameters reported herein (Table 2.1) are comparable to results for young humans (mean values of which are[15] $\{ c, c_1^1, c_2^1, c_1^2, c_2^2, c_1^{3,4}, c_2^{3,4}, \alpha_o \}$ = {19.34 kPa, 2.37 kPa, 1.48, 4.70 kPa, 0.59, 11.87 kPa, 0.87, 41.8 deg}). Nevertheless, it was found that, in comparison to the suprarenal aorta, the infrarenal aorta had a slightly lower material stiffness, which when combined with its lower thickness and similar axial prestretch might suggest a lower structural stiffness. Yet, such a conclusion would be in contrast to the aforementioned *in vivo* measurements of distensibility and cyclic strain (Amirbekian et al., 2009; Goergen et al., 2011), thus suggesting possible differences in perivascular tethering above and below the level of the renal arteries, which was not evaluated herein. Albeit often not considered in most biomechanical models, there is clearly a need to

understand better and then account for aortic perivascular tethering (which is not axisymmetric) in future models of the aorta and the subsequent development of aneurysms. Indeed, our results necessarily yielded mean properties since diameters were measured anterior to posterior, which does not allow one to delineate possible circumferential differences due to possible perivascular support on the posterior aspect. Similarly, we focused on responses within the central region of each specimen, away from branches. There is also a need to understand possible regional heterogeneities associated with branch sites. Finally, we focused on young male mice. There is a need to quantify the effects of aging, which could differ in these two regions of the abdominal aorta, and to quantify possible gender related differences, particularly because AAAs tend to occur more often in males than females. Regardless, it is hoped that the present novel results on aortic material behaviors will provide a foundation for and stimulate much needed modeling of aneurysmal progression in diverse mouse models of AAAs.

CHAPTER III

MECHANICAL EFFECTS OF ELASTASE ON THE PROPERTIES OF THE INFRARENAL ABDOMINAL AORTA: IMPLICATIONS FOR ABDOMINAL AORTIC ANEURYSM MODELS IN MICE

Overview

Intraluminal exposure of the infrarenal aorta to porcine pancreatic elastase is one of the more commonly used, targeted, models for AAA development. The *in vivo* effects of elastase exposure have been well documented in multiple animal models. Understanding the mechanical effects *in vitro* of the acute loss of elastin may provide additional insight into this particular model as well as into aneurysm development as a whole. In this paper, we present the first biaxial mechanical data and nonlinear constitutive descriptors for the post-elastase infused infrarenal aorta. These data reveal a significant change in the behavior of the vessel as a whole. Such data promises to help better understand the effects of the loss of elastin on the behavior of the aorta during aneurysm development.

Introduction

Abdominal Aortic Aneurysms (AAAs) are the 13th leading cause of death in the United States and the 10th leading cause in men over the age of 55. With an increasing size of an aging population, these numbers are expected to rise. For this reason, there has been a heightened interest in understanding the mechanics and the pathophysiology of AAAs. The most conspicuous change in an aneurysmal aorta is the loss of functional

elastin. Elastin is highly important structural component of the arterial wall and it normally has a long half-life. The high percentage of elastin gives the aorta its ability to effectively dampen the pulsatility of the blood.

Several experiments have focused on *in vivo* effects of elastase infusion on rat aortas (Anidjar et al., 1990; Anidjar et al., 1994), dog carotids (Dobrin and Canfield, 1984; Dobrin and Grey, 1985), rabbit carotids (Fonck et al., 2007), mouse carotids (Ferruzzi et al., 2011) and mouse aortas (Goergen et al., 2011; Thompson et al., 2006). The aorta studies have focused on the effects on the diameter and histology of the vessels. Surprisingly, only the studies of Fonck et al. (2007) and Ferruzzi et al. (2011) looked at changes in mechanical effects following subsequent growth and remodeling. In this study, we focus on the acute damage done to and associated changes in mechanical properties of an aorta after a sudden loss of functional elastin.

Methods

Specimen Preparation. Animal care and use was approved by the Texas A&M University Institutional Animal Care and Use Committee and followed methods used previously in our laboratory (cf. Dye et al., 2007; Eberth et al., 2009b). Briefly, following an overdose of sodium pentobarbital, the infrarenal abdominal aorta was excised from 8-12 week old male mice. The tissue was trimmed of all excess perivascular tissue, cannulated using custom glass pipettes, and secured to the cannulae using 6-0 silk suture. Branches were either ligated with suture or blocked using microspheres to enable the specimen to be pressurized when mounted in the testing

device. The chamber was filled with Dulbecco's Phosphate-Buffered Saline (DPBS) with calcium (Invitrogen) and maintained at 37 degrees Celsius.

Mechanical Testing. The infrarenal aortas from previous work were used as our control data. These vessels underwent an initial testing protocol involving determination of unloaded measurements, acclimation, preconditioning, and mechanical testing consisting of pressure-diameter and force-length protocols. Unloaded dimensions were recorded using a video-microscope. Acclimation to pressure (80 mmHg) and the nearly *in vivo* axial stretch for 15 minutes was followed by preconditioning via 3 cycles of pressurization from 10-140 mmHg. Unloaded data were collected again, this time at a pressure of 5 mmHg to avoid collapsing the vessel; there was typically minimal increase in dimensions relative to those taken prior to acclimation and preconditioning. Pressure-diameter testing involved cyclically pressurizing the vessel from 10-140 mmHg while holding it at a constant stretch of *in vivo* and ± 5% of the *in vivo* stretch. The force-length protocol involved cyclically stretching the vessel from 0 to 1.5 g force while maintaining a pressure of 60, 100, and 140 mmHg.

After this initial mechanical test was completed, 3 mL of elastase (9.5 U Elastase/mL DPBS) was delivered intraluminally and was allowed to take effect for 30 minutes, in the presence of 100 mg/L calcium chloride and held at a temperature of 37°C. Once the change in outer diameter approached zero, typically within 20 minutes, it was assumed that maximal effects had taken place. The new unloaded diameter and length were measured and the post-elastase "*in vivo*" stretch was determined based on the stretch at which the force remained nearly constant with increasing pressure. A

second mechanical test was run using the new "*in vivo*" stretch as well as values corresponding to 5% above. The values from the 5% below "*in vivo*" were generally unusable due to the force being at or below zero for the entirety of the test.

Constitutive Modeling. This biaxial data were then used to quantify the associated mechanical behavior. The data were converted to mean circumferential and axial Cauchy stresses using standard formulas (Humphrey 2002)

$$t_{\theta\theta}^{exp} = \frac{P^{exp}a}{h}, \;\; t_{zz}^{exp} = \frac{f^{exp}}{\pi h(2a+h)} \tag{3.1}$$

where a is the inner radius in any loaded state and h is the associated thickness of the wall. The former was calculated using wall volume

$$V = \pi(B^2 - A^2)L \;\; , \;\; a = \sqrt{b^2 - \bar{V}/(\pi l)}, \tag{3.2}$$

which in turn allowed wall thickness to be computed easily ($h = b - a$). The applied axial force on the artery is given by $f^{exp} = f_T^{exp} + \pi a^2 P^{exp}$, where f_T^{exp} is measured by the force transducer and P^{exp} is measured by the pressure transducer.

Briefly, a 2D model "four-fiber family" hyperelastic constitutie model (Ferruzzi et al., 2011) was used, assuming that the radial component of stress was negligible. This model has proven useful in capturing biaxial mechanical responses of diverse mouse arteries (Eberth et al., 2009b; Gleason et al., 2008; Wan et al., 2010). Thus, a strain-energy function of the following format was employed:

$$W = \frac{c}{2}(I_c - 3) + \sum_{k=1-4} \frac{c_1^k}{4c_2^k}\{exp[c_2^k((\lambda^k)^2 - 1)^2] - 1\} \tag{3.3}$$

$$I_c = \lambda_r^2 + \lambda_\theta^2 + \lambda_z^2 \tag{3.4}$$

$$\lambda^k = \sqrt{\lambda_\theta^2 sin^2\alpha^k + \lambda_z^2 cos^2\alpha^k} \tag{3.5}$$

$$\{\alpha^1 = 0,\ \alpha^2 = \pi/2\,, \alpha^3 = \alpha^{-4}\} \tag{3.6}$$

where α^k is the angle of the k[th] fiber family with respect to the axial direction and the constants c, c_1^k, and c_2^k are material parameters found via nonlinear regression.

Best-fit values of the unknown parameters in equation (3.3) were determined using a nonlinear least squares minimization of the error e between the theoretically predicted (*theory*) and experimentally inferred (*exp*) applied loads, namely

$$e = \sum_1^N \left[\left(\frac{P^{theory} - P^{exp}}{P^{avg}}\right)^2 + \left(\frac{F^{theory} - F^{exp}}{F^{avg}}\right)^2\right]_i \tag{3.7}$$

where N is the total number of data points (i.e., equilibrium configurations) for all experimental protocols combined for each specimen and *avg* denotes the overall average value. The error e was minimized using the built-in function *lsqnonlin* in MATLAB, subject to physical constraints that $c, c_{1,}^i c_2^i \geq 0$ and $0 \leq \alpha_o \leq \pi/2$ due to the symmetry of the diagonal fibers.

Histology. All vessels were fixed in 4% formalin in an unloaded state for 1 hour, then immersed in cryoprotectant (30% sucrose) overnight. They were placed in optimum cutting temperature medium in 2-methylbutane cooled with liquid nitrogen and stored at -80^{o}C. Frozen samples were sectioned at 5 μm and stained with hematoxylin and eosin (H&E) to identify cell nuclei and Verhoeff-Van Gieson (VVG) to identify elastin.

Results

The most notable changes to the aorta following infusion of elastase were the visual increase in vessel diameter and the associated rightward shift of the pressure-

diameter data between the native infrarenal aorta and the same vessel after brief exposure to elastin (Figures 3.1 and 3.2). Exposure to elastase resulted in non-uniform dilation of the vessels.

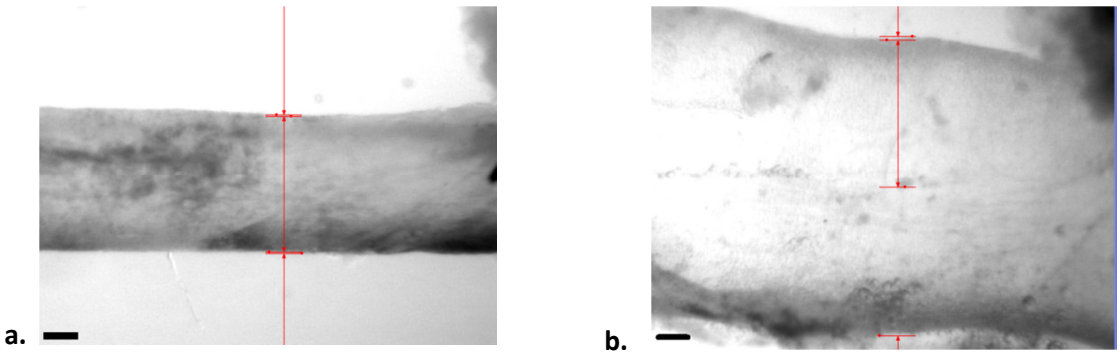

Figure 3.1. Video-microscope images of the infrarenal aorta mounted within the test device at 100 mmHg and its normal value of *in vivo* stretch both before (a) and after (b) a 30 minute exposure to elastase. Note the dramatic acute dilation.

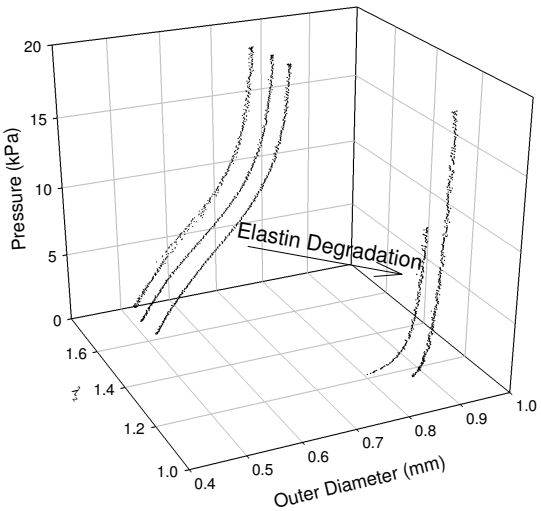

Figure 3.2. Pressure-diameter data collected at multiple values of axial stretch before and after exposure of the infrarenal aorta to elastase. Note the dramatic rightward shift in the pressure-diameter response and the much lower values of axial stretch following exposure to the elastase.

Figure 3.3 shows representative results for the fit of the constitutive model to pressure-diameter and pressure-force data; for clarity in presentation, the data were culled from the original files that were used in the nonlinear regressions. Note that the elastase resulted in a marked loss of distensibility relative to that expected of an elastic vessel like the aorta. The fits to the data for the elastase-treated vessels were not as good as those found for native vessels (e_{avg_native} = 8.69 ± 5.83 as compared to $e_{avg\_elastase}$ = 94.56 ± 76.93). Table 3.1 lists the best-fit model parameter for the equation 3.3. It has been suggested (Ferruzzi et al., 2011) that the median values of the parameters may better represent the overall mean behavior of the vessels, hence note that median values of the parameters following treatment with elastase were c = 6.02 E-07 kPa, c_1^1 = 154.78 kPa, c_2^1 = 1.45 E-89, c_1^2 = 1.69 E-06 kPa, c_2^2 = 0.24, c_1^3 = 0.60 kPa, c_2^3 = 3.85, and angle = 47.09 degrees. The dramatically reduced value of the best-fit parameter *c,* which models for elastin in the vessel wall, suggested a nearly complete loss of elastin when compared to the native vessel.

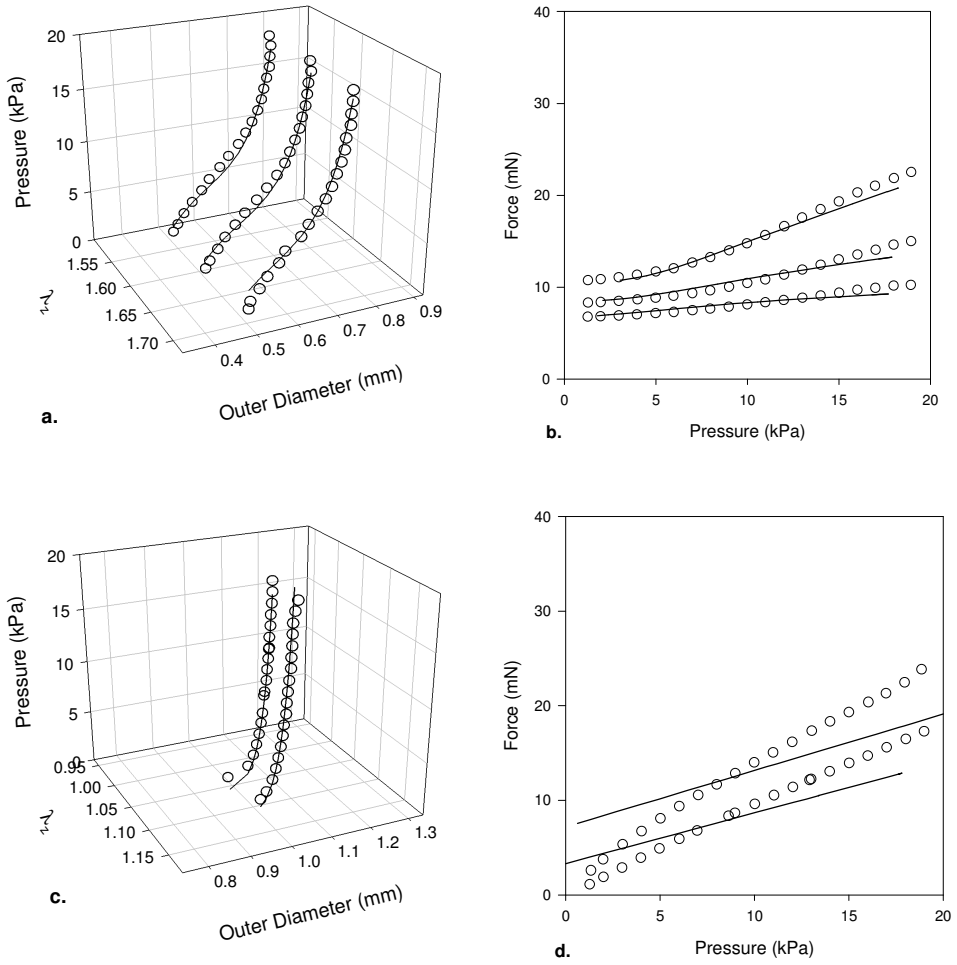

Figure 3.3. Pressure-diameter and pressure-force for the native vessel (a and b) as compared to the pressure-diameter and pressure-force data for the post-elastase vessel (c and d). Culled data are represented by the symbols and the best-fit model by the solid lines. Note the decrease in distensiblity and increase in force on the vessel. Note, too, that the scales are different for the untreated and elastase-treated aorta.

Table 3.1. Best-fit values (mean ± standard deviation) for parameters in the constitutive model given in equation 3.3 for all elastase-treated infrarenal aorta specimens. For comparison, best-fit mean values are also listed for untreated infrarenal aortas based on results from Chapter II.

		AXIAL		CIRCUMFERENTIAL		DIAGONAL		
Vessel	c (kPa)	c_1 (kPa)	c_2	c_1 (kPa)	c_2	c_1 (kPa)	c_2	angle (deg)
1	6.04E-06	1.62E-08	0.06	80.70	38.41	104.16	3.85	18.98
2	2.22E-14	2.29E-14	0.06	28.90	360.25	54.49	142.22	48.05
3	6.02E-07	154.78	1.65E-12	1.69E-06	8.25E-09	0.45	3.81	47.09
4	2.22E-07	201.60	1.45E-08	1.66E-10	1.27E-10	0.60	4.76	49.81
5	7.75E-05	167.34	3.08E-09	3.79E-09	2.41E-01	0.45	2.65	43.16
Mean ± SD	1.69E-5 ± 3.40E-5	104.74 ± 97.14	2.48E-2 ± 0.03	21.92 ± 35.16	79.78 ± 157.66	32.03 ± 46.61	31.46 ± 61.92	41.42 ± 12.78
Native ± SD	5.84 ± 1.82	6.21 ± 3.76	0.27 ± 0.31	4.77 ± 2.73	0.32 ± 0.17	1.22 ± 0.60	1.45 ± 0.80	37.98 ± 1.99

The unloaded outer diameter increased by 1.44 ± 0.32 fold and the unloaded length increased 1.46 ± 0.13 fold. VVG staining confirmed that these changes were due primarily to the loss of elastin (Figure 3.4). These geometric and microstructural changes manifested in the mechanical tests. For example, *in vivo* axial stretch decreased from 1.49 ± 0.16 to 1.06 ± 0.04 and the circumferential stress-stretch behavior exhibited an extreme stiffening around a much larger diameter (Figure 3.5) following exposure to elastase. After elastase exposure the infrarenal aorta appears to maintain some of its material symmetry in regards to the circumferential stresses when calculated for the equibiaxial stretch related Cauchy-stress (Figure 3.6). Table 3.2 provides information on

individual mice, noting that unloaded wall thickness was measured using rings taken from the native vessel whereas it was calculated based on the assumption of isochoric (volume conserving) deformations for the elastase-treated vessels. All differences in parameters reported in Table 3.2 for vessels before and after exposure of elastase were statistically significant with a $p < 0.01$ (t-test).

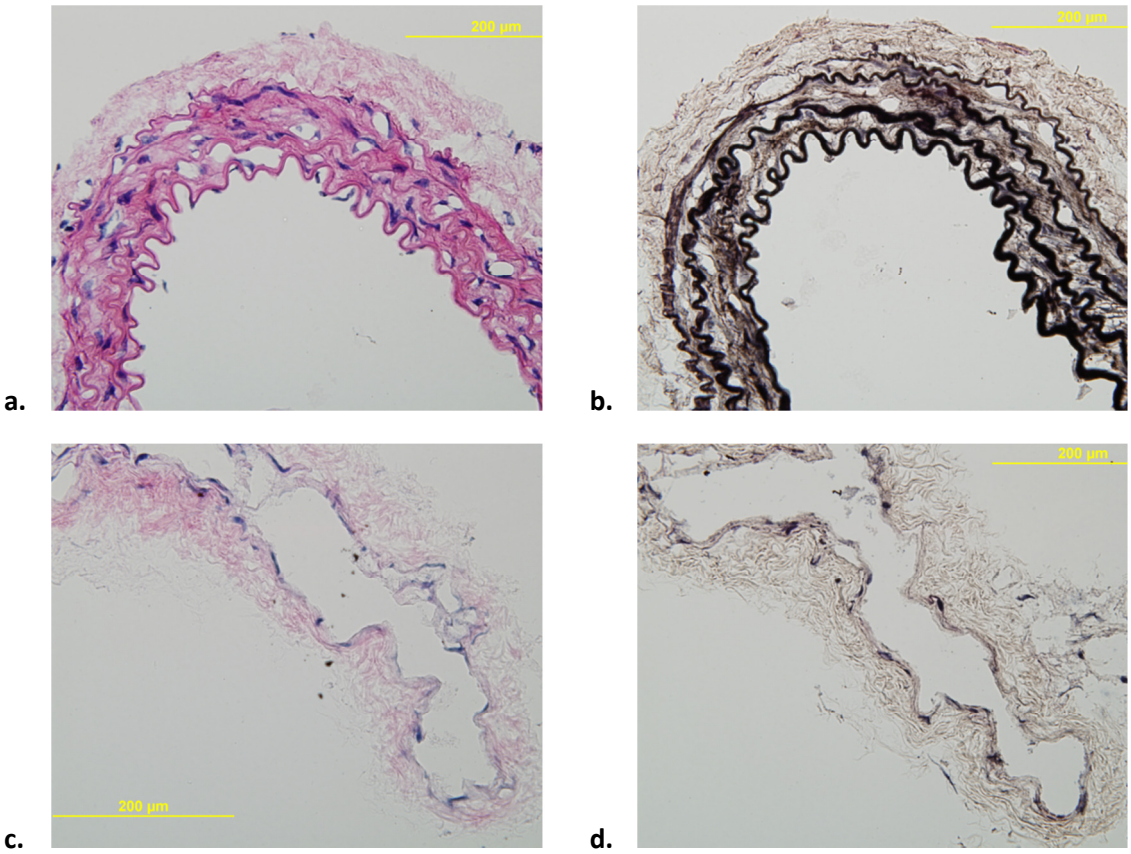

Figure 3.4. H&E stain for elastin in the native (a) and post-elastase vessel (c). Collagen is stained in pink and cell nuclei in purple. VVG stain for elastin in the native (b) and post-elastase vessel (d), where elastin is stained black.

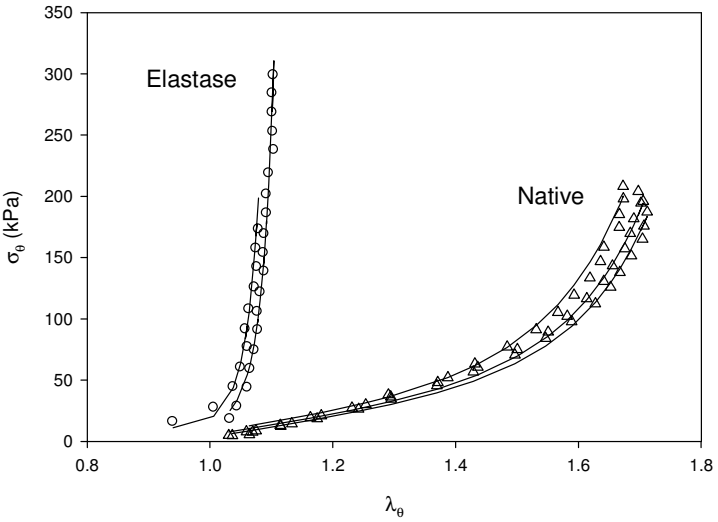

Figure 3.5. Comparison of circumferential Cauchy stress-stretch behaviors (symbols) for representative native and elastase-treated infrarenal aorta and the associated predictions (solid curves) based on the equations 3.3 and best-fit values of parameters listed in Table 3.1. Note the marked decrease in circumferential distensibility and increase in circumferential stiffness following treatment with elastase.

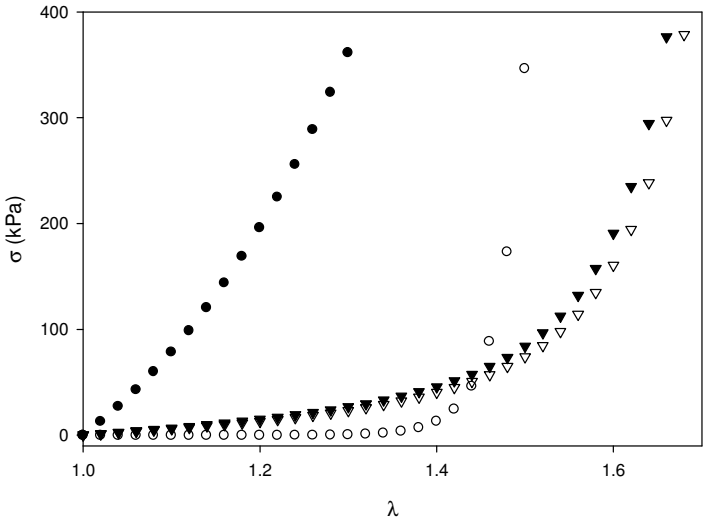

Figure 3.6. Comparison of equibiaxial stretch related Cauchy stress-stretch curves. Plotted are the elastase treated vessels (circles) and native vessels (triangles) for both the circumferential stresses (open symbols) and axial stresses (closed symbols).

Table 3.2. Mean values of relevant data on age, weight, and geometry of the native and post-elastase infrarenal aorta. Note that the length, outer diameter, and thickness are given in the unloaded configuration. An * denotes statistical differences at $p < 0.01$.

Vessel	Age (wks)	Weight (g)	lambda (--)	l_o (mm)	OD_o (um)	H_o (um)	**a** (um) @80 mmHg	**h** (um) @80 mmHg
Native	9.7 ± 0.8	21.8 ± 2.5	1.49 ± 0.16 *	3.35 ± 0.65 *	523 ± 46 *	88.8 ± 9.7 *	303 ± 29 *	40.0 ± 7.0 *
Elastase	9.8 ± 0.9	23.4 ± 1.6	1.06 ± 0.04 *	4.42 ± 0.71 *	722 ± 182 *	39.0 ± 10.5 *	482 ± 48 *	23.8 ± 2.1 *

Discussion

Aging causes marked decreases in the structural integrity and biological function of elastin, which in turn appears to contribute to the initiation or progression of multiple vascular diseases (e.g. hypertension, atherosclerosis, and aneurysms). In order to better understand mechanical consequences of the acute loss of functional elastin, we exposed otherwise normal mouse infrarenal aorta to a 30-minute intraluminal infusion of pancreatic elastase. This protocol was selected based on pilot data and results from prior studies. The geometry, microstructure, and mechanical properties of all aortas were dramatically different after exposure to elastase, similar to reports on the effects of elastase on other arteries from various species. Dobrin et al. (1984), Fonck et al. (2007), and Feruzzi et al. (2011) also reported that elastase causes a dramatic dilatation, especially at low pressures, and marked circumferential stiffening of normal carotid arteries from dogs, rabbits, and mice, respectively. Fonck and colleagues reported further that elastase does not alter the amount of fibrillar collagen within the wall, but it causes a slight thinning of the wall, a modest increase in overall length (~ 10%), and a dramatic decrease in the residual stress related opening angle. These findings are qualitatively

consistent with our results, but quantitatively different. We found a much greater thinning of the wall (~59% decrease in wall thickness; cf. Figure 3.3 and Table 3.2) and increase in the unloaded length (~46%). One reason for different results is that elastin constitutes a much greater percentage of the extracellular matrix in the aorta than carotid vessels, thus effects of removing elastin should be expected to be more dramatic in the aorta. For example, canine abdominal aortas consist of 30.1 ± 1.7 % elastin whereas their carotid arteries consist of 20.1 ± 1.0% elastin (Humphrey 2002). Although the percentages are different in mice (~28% as found in our previous infrarenal study) the same generalization is true; the carotids have a lower elastin to collagen ratio than aortas and thus less pronounced dilatation, extension, and stiffening.

Our findings on elastase-induced changes in the values of the material parameters for elastin-dominated and collagen-dominated contributions to overall wall properties (Tables 3.1 and 3.2) suggest a strong coupling of these major structural proteins. The highly pre-stretched elastin increases the undulation of collagen at low loads and thus contributes to the characteristic gradual stiffening of normal arteries over a broad range of stretches (Ferruzzi et al., submitted). Loss of elastin thus affects the initial undulation of collagen fibers at lower loads and consequently their stiffening character at increased stretch. Similarly, Fonck et al. (2007) noted that rabbit carotids treated with elastase had a rapid diameter increase below 25 mmHg and then diameter remained relatively unchanged. This was attributed to a substantial amount of the collagen fibers being fully engaged.

Because of the acute loss of elastin without adaptive growth and remodeling, the collagen fibers and smooth muscle cells would be expected to experience a stress other than homeostatic. Since our model does not capture the coupled effects of elastin, collagen, and smooth muscle cells, pressure-diameter and pressure-force fits are less accurate that what we see in vessels that have had a chance to remodel. Our model assumes a certain degree of undulation in the collagen fibers, which, due to the large increase in unloaded length, is unlikely to be the case. This has been shown previously in our lab to be the case with carotids (Ferruzi et al., 2011). Rezakhaniha et al. (2011) suggested a move from the commonly assumed isotropic behavior of elastin to modeling elastin as another anisotropic contributor to overall wall mechanics. This change allowed for better fits to their rabbit carotid elastase-treated pressure-diameter and pressure-force data.

Abdominal aortic aneurysms are caused by dramatic changes in the microstructure of the wall of the aorta. One of these changes is a marked elastin fragmentation. For this reason, *in vivo* infusion of elastase is a common model for AAA development. In these studies, elastase is applied intraluminally to the infrarenal aorta for a short period. Generally a mild initial dilatation is seen, followed 7-10 days later by a significant increase in outer diameter and macrophage activity (Thompson et al., 2006). The mechanisms of this are not fully understood, but the sudden, drastic change in the vessel geometry (extending, dilating, as well as a decrease in force exerted on the vessel) obviously play a role in the subsequent days and weeks. Although numerous studies investigate the biology and implicate a change in mechanics in AAA models in

mice (Ailawaadi et al., 2009; Cassis et al., 2009; Daugherty and Cassis, 2004; Deguchi et al., 2009; Goergen et al., 2011; Saraff et al., 2003), there has been little attention to the biaxial mechanical properties brought about by the individual changes in the microstructure. Here we present biaxial mechanical data that may help explain both the effects of functional elastin on the mechanical behavior of the infrarenal aorta as well as the initial behavior of AAA development in elastase models.

In summary, we found that treatment of infrarenal aortas with porcine pancreatic elastase resulted in large, non-uniform dilation and extension. In the acute situation, the dilatation was sub-aneurysmal (i.e., 44%, not greater than 50% which is the general rule of thumb), but the arteries did exhibit stiffening and a decrease in distensibility that are characteristic of AAAs. This work presents the first biaxial data with constitutive descriptors for elastase-treatment of infrarenal aortas. These findings should provide interesting insights into the mechanics of the evolving AAA, especially in the *in vivo* elastase model.

CHAPTER IV

QUANTIFICATION OF THE MECHANICAL PROPERTIES OF THE SUPRARENAL AORTA IN SMOOTH MUSCLE α-ACTIN WILD-TYPE, HETEROZYGOUS, AND NULL MICE

Overview

Mutations in the gene encoding for α-smooth muscle actin have been discovered in patients with thoracic aortic aneurysms and dissections. Amongst possibly other effects, this mutation appears to alter the normal phenotypic modulation of the smooth muscle cells as well as to disrupt the smooth muscle cell's ability to contract and thereby to contribute directly to the normal regulation of blood flow. There has not been any study, however, of possible consequences of mutations in α-smooth muscle actin on overall arterial mechanical properties. Hence, we report here the first comparison of biaxial mechanical behavior and constitutive relations for the suprarenal aorta in the α-smooth muscle actin wild-type, heterozygous, and null mice.

Introduction

Studies of human subjects having thoracic aortic aneurysms and dissections (TAAD) have revealed a mutation in the ACTA2 gene (Guo et al. 2007) which encodes alpha-Smooth Muscle Actin (αSMA). αSMA is the most abundant protein in adult vascular smooth muscle cells. In a normal cell, the thin actin filaments interact with the thicker myosin fibers in the presence of calcium to cause the cell to contract. It is not surprising, therefore, that loss of function αSMA results in decreased contractility of

blood vessels (Schildmeyer et al., 2000). In addition, however, aortic tissue from patients having ACTA2 mutations showed fragmentation and loss of elastin fibers and decreased smooth muscle cell density, indicative of medial degeneration (Guo et al., 2007). Conversely, internal carotid arteries from these patients show signs of inward remodeling and obstructive blood flow characteristic of Moyamoya disease (Milewicz et al., 2010). It thus appears that αSMA is important for a myriad of cell functions.

Despite the importance of smooth muscle cell contractility to arterial vessel behavior, there has been little research to quantify the effects of αSMA mutations on either the active or passive mechanical properties of arteries. The primary work done to date has used uniaxial ring tests to assess changes in wall mechanics (Schildmeyer et al., 2000). Although such tests are useful for qualitative comparisons, ring tests do not reflect the biaxial mechanical behaviors that are important *in vivo*. In this study, therefore, we report the first biaxial data on the passive mechanical behavior of the aorta due to αSMA mutations. Toward this end, we used an αSMA heterozygous mouse developed by Dr. Robert Schwartz at the Baylor College of Medicine to generate wild-type (+/+), heterozygous (+/-), and homozygous null (-/-) mice from which we excised the suprarenal aorta for biaxial mechanical testing.

Methods

Specimen Preparation. All protocols were approved by the Texas A&M University Institutional Animal Care and Use Committee (IACUC). Male mice between the ages of 8 and 12 weeks of age used for each of the three mouse models (+/+, +/-, and -/-). Mice were euthanized using a lethal intra-peritoneal (IP) injection of sodium

pentobarbital (250 mg/kg) and an incision was made from the tail to the chest to expose the abdominal cavity including the aorta. The suprarenal aorta was isolated and excised via two incisions, one just below the diaphragm and another between the renal arteries. The aorta was then placed in warm Hanks Balance Salt Solution (HBSS) containing calcium, branches were tied off using 7-0 silk suture, and the vessel was cannulated on custom-pulled glass cannulae, and secured using 6-0 silk suture.

Mechanical Testing. Specimens were submerged in a temperature-controlled chamber with circulating HBSS containing calcium. A peristaltic pump provided flow to both the adventitial bath and the luminal flow loop. Luminal pressure was controlled by regulating the air-CO_2 pressure on the surface of the luminal reservoir. A side-mounted CCD camera measured vessel outer diameter, while precision stepper motors controlled the length of the specimen. Attached to the distal cannula, a force transducer measured the applied axial force. Further detail on the experimental set-up can be found in Gleason et al (2004). Information on the unloaded dimensions was obtained interactively by determining the length at which the vessel first bent when unloaded at zero pressure. From this unloaded length, we calculated the axial stretches during testing. The vessel was stretched to a near *in vivo* (λ_z^{iv}) value for preconditioning. The preconditioning protocol involved 3 cycles of pressurization from 10-140 mmHg to minimize hysteresis. Then, we determined the *in vivo* stretch of the individual vessel by finding that stretch at which the axial force did not change with pressurization. The computer then ran a pre-programmed routine to achieve various axial stretch and pressure set-points. In testing such as this, volume ($\bar{V}$) remains constant, thus values of

the inner radius can be calculated from the experimentally measured outer radius and axial stretch using the incompressibility constraint (Humphrey, 2002; Wicker et al., 2008), namely:

$$a = \sqrt{b^2 - \bar{V}/(\pi l)} \qquad h = b - a \qquad (4.1, 4.2)$$

The mechanical testing routine consisted of (i) cyclically pressurizing the specimen from 10 mmHg to 140 mmHg twice at three fixed axial stretches (*in vivo*, -5% *in vivo*, and +5% *in vivo*) and (ii) cyclically loading the vessel axially from 0 to 24.5 mN (2.5 g) three times while holding the pressure constant at 60mmHg, 100 mmHg, and 140 mmHg.

Histology. After mechanical testing was completed, vessels were removed from the testing device, fixed in 4% formalin in an unloaded state for 1 hour, and then immersed in cryoprotectant (30% sucrose) overnight. They were then placed in optimum cutting temperature medium in 2-methylbutane cooled with liquid nitrogen and stored at -80^{o}C. Frozen samples were sectioned at 5 μm and stained with Verhoeff-Van Gieson (VVG) to identify elastin, Movat's Pentachrome to identify elastin, collagen, fibrin and muscle cells, Caldesmon to identify smooth muscle cells, and alpha-Smooth Muscle Actin (α-SMA) Antibody to confirm the presence or absence of α-SMA.

Constitutive Modeling. Stress is a key mediator of growth and remodeling of the arteries, thus it is an important measure. Using a 2D approach, mean values of the Cauchy stress in circumferential ($\sigma_{\theta\theta}$) and axial (σ_{zz}) directions are defined by (Humphrey, 2002; Gleason and Humphrey 2005):

$$\sigma_{\theta\theta} = \frac{Pa}{b-a} \qquad \sigma_{zz} = \frac{f_T + \pi a^2 P}{\pi h(2a+h)} \tag{4.3, 4.4}$$

where P is the transmural pressure, f_T the force measured by the force transducer, and b and a being the outer and inner radii of the loaded vessel. Values of stretch were calculated based on the unloaded configuration and by using mid-wall radius values ($r_{mid} = (b-a)/2$).

$$\lambda_\theta = \frac{r_{mid}}{R_{mid}} \qquad \lambda_z = \frac{l}{L} \tag{4.5, 4.6}$$

where R_{mid} and L are the unloaded mid-wall radius and unloaded length respectively and l is the current length.

To quantify the passive biaxial behavior exhibited by the suprarenal aorta, we employed a four-fiber family stain-energy equation (Baek et al., 2007):

$$W = W_{iso} + W_{aniso} \tag{4.7}$$

$$W_{iso} = \frac{c}{2}(I_c - 3) \tag{4.8}$$

$$W_{aniso} = \sum_{k=1-4} \frac{c_1^k}{4c_2^k}\{exp[c_2^k((\lambda^k)^2 - 1)^2] - 1\} \tag{4.9}$$

$$\lambda^k = \sqrt{\lambda_\theta^2 sin^2\alpha^k + \lambda_z^2 cos^2\alpha^k} \tag{4.10}$$

$$\{\alpha^1 = 0,\ \alpha^2 = \pi/2\,, \alpha^3 = \alpha^{-4}\} \tag{4.11}$$

where I_c is the first invariant of the right Cauchy-Green tensor, α^k is the angle of the k^{th} fiber family with respect to the axial direction, and the constants c, c_1^k, and c_2^k are material parameters found via nonlinear regression.

Best-fit values of the parameters were calculated using a nonlinear regression (MatLab's lsqnonlin function) to minimize the following objective function:

$$e = \sum_1^N \left[\left(\frac{\left(P^{Theory} - P^{Exp}\right)_i}{\tilde{P}^{Exp}} \right)^2 + \left(\frac{\left(F_v^{Theory} - F_v^{Exp}\right)_i}{\tilde{F}_v^{Exp}} \right)^2 \right] \quad (4.12)$$

where the superscript "Theory" denotes values calculated using equations 4.7-4.11 and superscript "Exp" denotes values that were measured directly, with F_v the net axial force on the vessel, defined by $f_v = f_T + \pi r_i^2 P$, $\tilde{P}$ and $\tilde{F}$ are average values of pressure and force measured experimentally.

Results

Animals in each of the three groups were of similar age and weight, and they had similar values of *in vivo* axial stretch (Table 4.1). Wild-type (+/+) mice averaged 9.4 weeks, 26.1 grams, and 1.34 stretch, heterozygous (+/-) mice averaged 9.9 weeks, 26.9 grams, and 1.41 stretch, and knockout (-/-) mice averaged 10.6 weeks, 25.3 grams, and 1.38 stretch. None of the values in Table 4.1 were statistically significant ($p<0.05$), Table 4.2 lists best-fit values of the material parameters for the (+/+), (+/-), and (-/-) mice.

Table 4.1. Mean values of relevant data on age, weight, and geometry of the wild-type (+/+), heterozygous (+/-), and homozygous null (-/-) mice and the excised suprarenal aorta. Note that the length (l_o), outer diameter (OD_o), and thickness (H_o) are given in the unloaded configuration.

Vessel	**Age** (wks)	**Weight** (g)	**LAMBDA** (--)	**l_o** (mm)	**OD_o** (um)	**H_o** (um)	**a (um)** @80 mmHg	**h (um)** @80 mmHg
+/+	9.4 ± 0.8	26.1 ± 1.5	1.34 ± 0.06	4.51 ± 0.37	792 ± 24	99 ± 20	508 ± 32	50 ± 4
+/-	9.9 ± 0.9	26.9 ± 1.7	1.41 ± 0.08	4.70 ± 0.98	799 ± 44	96 ± 5	504 ± 29	48 ± 4
-/-	10.6 ± 1.1	25.3 ± 2.2	1.38 ± 0.16	4.28 ± 0.61	802 ± 45	101 ± 14	498 ± 52	50 ± 6

Pressure-diameter and pressure-force data and associated fits to data using the four-fiber family constitutive model are shown in Figure 4.1; for purposes of increased clarity in presentation, these data were culled from those used in the nonlinear regression. As it can be seen from Figure 4.1, the (+/-) mice have a more pronounced sigmoidal shape to the pressure-diameter curve. This finding could suggest a higher elastin-to-collagen ratio in these vessels. Indeed, results in Table 4.1 suggest that, albeit not statistically significant, there was also a trend toward higher values of the *in vivo* axial stretch in the (+/-) mice. It is thought that increased elastin to collagen ratios associate with larger *in vivo* axial stretches (Eberth et al., 2009a; Humphrey et al., 2009). Panels b and d in Figure 4.1 and a in Figure 4.2 reveal further that similar forces were found at similar stretches. Assuming that the aorta attempts to achieve and maintain homeostatic values of stress (Humphrey, 2008), this would suggest similar cross-

sectional areas at similar *in vivo* stretches. To test this, we used the mean systolic blood pressure values reported in the literature (Schildmeyer et al., 2000) for the (+/+) and (-/-) mice of 114.4 mmHg and 82.2 mmHg respectively to calculate mean circumferential Cauchy stress (equation 4.3). We found, however, that at maximum values of systolic pressure, the (+/+) and (-/-) suprarenals had stress values of 31.1 ± 5.9 kPa and 44.8 ± 11.8 kPa respectively, which are statistically different ($p<0.05$).

Due to the difficulty in comparing overall behaviors based on values of multiple parameters in a nonlinear model, consider the strain energy predicted to be stored, per unit reference volume, at the same levels of pressure (from 60 to 120 mmHg) and the individual *in vivo* axial stretch (Figure 4.3). As it can be seen, the overall stiffness of the (+/-) aorta tended to be higher than that of the (+/+) and (-/-) aorta, especially at higher pressures. These differences were statistically significant, at a $p < 0.05$ (ANOVA) for the (+/+) and (+/-) vessels at a pressure of 120 mmHg.

Table 4.2. Best-fit values of model parameters (equation 4.7) for WT, Het, and KO suprarenal aorta specimens.

		Axial		Circumferential		Diagonal		
Vessel #	**c (kPa)**	**c_1 (kPa)**	**c_2**	**c_1 (kPa)**	**c_2**	**c_1 (kPa)**	**c_2**	**angle (deg)**
(+/+)								
1	9.43	29.25	0.49	10.79	0.13	2.01	3.30	31.58
2	20.24	8.98	0.35	12.10	7.84E-11	0.86	2.53	46.24
3	16.86	19.02	0.47	6.28	0.06	1.29	1.98	32.75
4	20.73	18.53	0.30	5.19	0.17	0.88	2.60	29.88
5	14.02	19.32	0.11	4.80	0.25	1.32	1.88	32.11
(+/-)								
1	28.13	12.77	0.44	3.38	0.50	0.61	3.08	30.31
2	21.44	19.40	0.17	5.51	0.24	0.47	3.02	31.69
3	9.78	27.04	0.10	9.42	0.16	1.57	2.75	31.08
4	23.33	14.39	0.16	6.04	0.24	0.49	1.94	28.52
5	19.24	15.06	0.26	7.57	0.46	0.85	2.57	32.05
6	23.04	24.09	0.15	3.41	0.52	1.05	2.93	31.41
(-/-)								
1	29.72	7.78	2.91	8.22E-05	4.06	2.24	2.86	41.08
2	21.61	12.34	0.51	5.46	0.47	0.91	2.71	34.03
3	0.97	10.93	0.12	6.58	0.39	4.93	0.73	27.62
4	21.11	13.91	0.09	11.10	0.77	0.89	1.53	32.26
5	18.01	52.13	1.64	3.22	0.61	0.68	16.99	24.40
6	24.68	17.55	0.19	2.89	0.56	0.53	2.17	30.98
Mean (+/+)	16.26 ± 4.69	19.02 ± 7.17	0.34 ± 0.15	7.83 ± 3.37	0.12 ± 0.10	1.27 ± 0.47	2.46 ± 0.57	34.51 ± 6.64
Mean (+/-)	20.83 ± 6.15	18.79 ± 5.76	0.21 ± 0.12	5.89 ± 2.36	0.35 ± 0.16	0.84 ± 0.42	2.71 ± 0.42	30.84 ± 1.28
Mean (-/-)	19.35 ± 9.84	19.11 ± 16.50	0.91 ± 1.14	4.88 ± 3.81	1.14 ± 1.43	1.70 ± 1.70	4.50 ± 6.17	31.73 ± 5.73

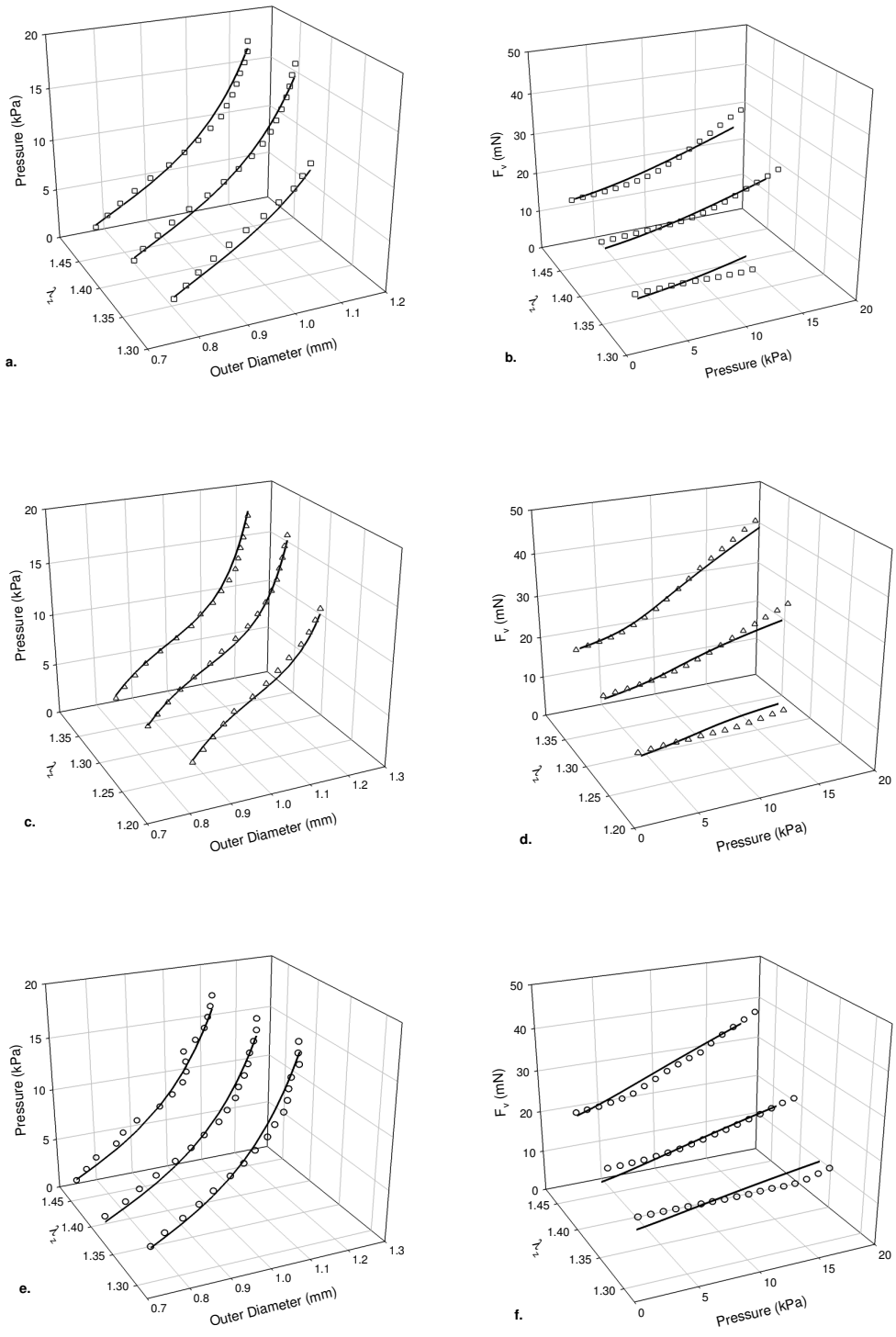

Figure 4.1. Representative pressure-diameter and pressure-force on the vessel data and fits. (+/+) (a and b), (+/-) (c and d), and (-/-) (e and f).

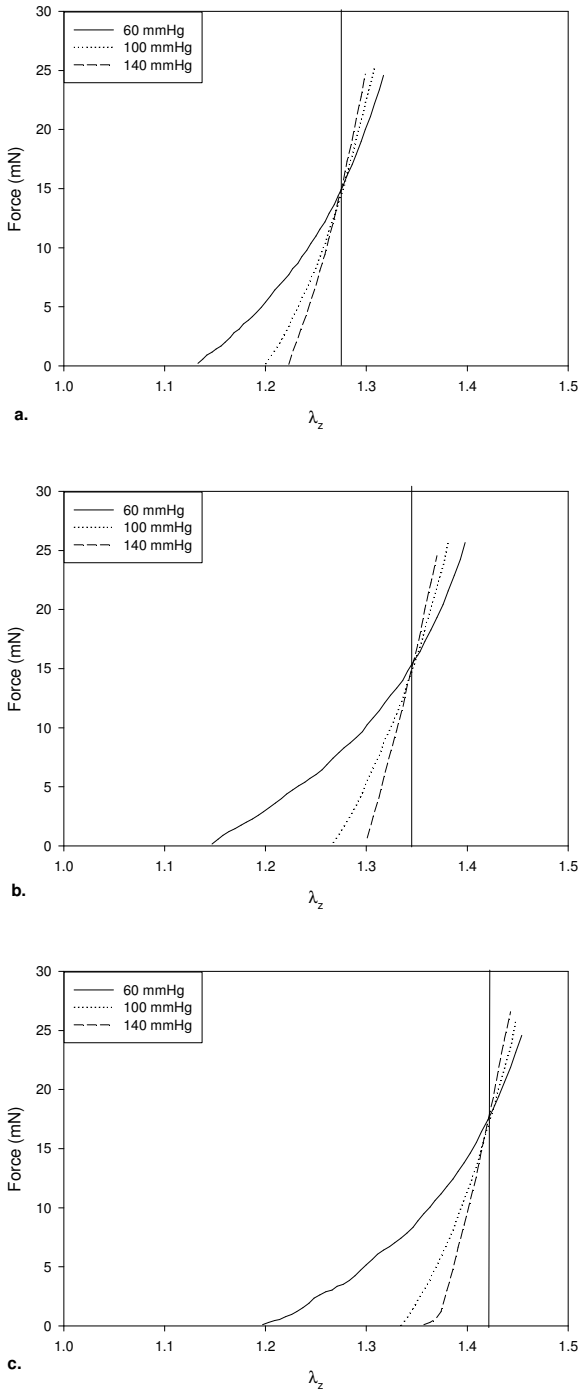

Figure 4.2. Representative force-length data for the (+/+), (+/-), and (-/-) mice (a, b, and c respectively). Note the similar force values at statistically similar *in vivo* stretches.

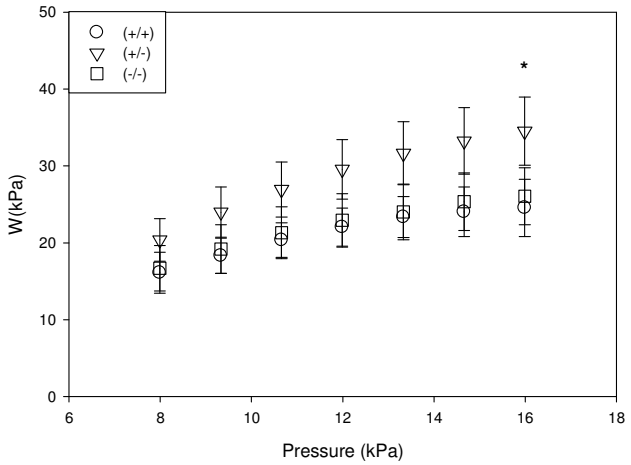

Figure 4.3. Mean values ± SEM of the computed strain energy stored in the (+/+) (circles), (+/-) (triangles) and (-/-) (squares) at different values of luminal pressure and the individual *in vivo* axial stretch. Note, * denotes a pressure at which the (+/-) value is statistically different than the (+/+) .

Discussion

Smooth muscle cell contractility is vitally important for muscular vessels. These vessels control blood flow in the body by constricting or dilating. Elastic vessels in mice, like the aorta, may experience minimal constriction and dilation in response to vasoconstrictors and vasodilators. Schildmeyer et al. (2000) found that the aorta of αSMA null mice had an up-regulation of skeletal α-actin. In that study, ring tests showed a decrease in contractility, but not a complete loss due to the presence of skeletal α-actin. The minimal necessity for contractility of the aorta *in vivo* as well as the up-regulation of skeletal α-actin may explain, in part, why the aorta shows little difference between wild type (+/+) and null (-/-) material parameters.

The major components of aneurysm formation are based on dramatic changes to the microstructure of the wall of the abdominal aorta. One of these changes is the

apoptosis of smooth muscle cells as well as the inability of the remnant smooth muscle cells to contract. Guo et al. (2007) reported an important finding that human subjects with thoracic aneurysms and dissections had mutation in the gene that encodes for αSMA. What they discovered was that aortic tissue experienced medial degeneration, areas of rapid SMC proliferation and disarray. In the vasa vasorum this proliferation caused stenosis of some vessels. When this is examined in combination with work looking at a myosin heavy chain mutation (Pannu et al., 2006) it became increasingly convincing that the ability of SMC to contract is important to the integrity of the aorta. However, the aorta does not contract biaxially, which may explain the discrepancy between the work by Pannu et a. (2006) and Guo et al. (2007) and this work, where we found similar mechanics between (+/+) and (-/-) vessels.

The importance found by these two groups is in stark contrast to the biaxial behaviors we observed in our mice. We noted no change in the wall thickness that would suggest proliferation of smooth muscle cells, nor did we find any evidence of medial degeneration. These differences are likely due to different responses of different vessels to similar genetic changes. For example, ACTA2 missense mutations in some human subjects are found to be related to familial thoracic aneurysms and dissections or to manifest as persistent livedo reticularis which is caused by occlusion of deep dermal capillaries (Guo et al., 2009). In some young patients (11 to 26 years of age), a mutation in αSMA lead to dilations of the aortic arch (Milewicz et al., 2010). In yet other patients, another missense mutation results in premature coronary artery disease

presenting with highly cellularized plaques, strokes, and Moyamoya disease in which there is an occlusion of the internal carotid arteries (Guo et al., 2009).

To this end, it does not appear that at such a young age, in an undisturbed environment, that the loss of smooth muscle cell function greatly affects the mechanical behaviors. This implies that the vasculature develops in such a way (with the replacement of αSMA with skeletal α-actin) that allows some arteries to function normally under normal conditions. There is a need to examine the effects of aging on the (+/-) and (-/-) arteries. The mechanical properties could become significantly different among the three groups examined here. For example, the suprarenal aorta of older αSMA null mice may become particularly susceptible to vascular abnormalities (specifically AAA) during infusion with an inflammatory agent (Angiotensin-II). It would also be beneficial to quantify the gender related differences in behavior, due to the fact that AAAs more commonly occur in males than females. The work presented here should provide a foundation for such future work.

CHAPTER V

THE EFFECTS OF ANGIOTENSIN-II ON THE MECHANICS OF THE SUPRARENAL ABDOMINAL AORTA OF THE APOE-/- MOUSE

Overview

Abdominal aortic aneurysm is a life-threatening disease that increasingly affects an aging population. One of the most common murine models of this disease is Angiotensin-II (Ang-II) infusion of atherosclerotic prone mice. In order to better understand the development of the Ang-II-induced AAA, it is necessary to understand the mechanics of the AAA produced. Here we present biaxial pressure-diameter and pressure-force data for AAAs after 28 days of Ang-II infusion.

Introduction

Abdominal aortic aneurysms (AAAs) are currently the 13th leading cause of death in the United States, presenting most often in older male patients. As the population continues to age, the incidence of AAA is expected to increase. AAAs are characterized by a loss of functional elastin, loss of smooth muscle cells function, and inflammation. Often times, these lesions associate with atherosclerotic plaque development and the enlarged lumen is the site of intramural thrombus.

There are three common mouse models for AAA, of which is motivated by roles of atherosclerosis, hypertension, and inflammation in the development of AAAs. This model uses a long-term subcutaneous infusion of angiotensin-II (Ang-II), often in the apolipoprotein-E null (ApoE-/-) mouse (Cassis et al., 2009; Deguchi et al., 2009).

Although Ang-II increases blood pressure, it primarily incites a significant inflammatory response that often leads to AAAs.

Several studies looked at various factors that either promote or inhibit AAA formation in the Ang-II infusion model. Zhang et al. (2009) determined that simvastatin (an HMG-CoA reductase inhibitor) inhibited AAA development and suggested that it may in part inhibit the ERK pathway (macrophage activation). Manning et al. (2003) found that the broad spectrum MMP inhibitor, doxycycline, reduced the incidence and severity of aneurysms. More recently, Goergen et al. (2011) found that the site of largest radius of curvature coincided with the location of AAA initiation.

Despite all of the biology being done to understand the pathways and possible pharmaceutical methods for slowing or reversing AAAs, there is one area that has not been analyzed. A complete understanding of the development of AAA due to Ang-II infusion must include an understanding of the change in the mechanics. In this paper, we present the first biaxial mechanical data of the suprarenal aorta of the ApoE -/- mouse after a 28 day Ang-II infusion.

Methods

Specimen Preparation. All animal protocols were approved by the Texas A&M University Institutional Animal Care and Use Committee. Two groups of ApoE-/- mice were used, ApoE-/- and ApoE-/- Ang-II infused mice. For the first group, suprarenal aortas were harvested and mechanically tested following methods previously utilized by our laboratory (cf. Dye et al., 2007; Eberth et al., 2009b).

The second group of ApoE-/- mice were obtained from Jackson Labs at eight weeks of age, anesthetized with inhaled isoflurane, and implanted with mini-osmotic pumps (Alzet, 1004) that were placed sub-cutaneously in the mid-scapular region. The pumps released Angiotensin-II (Sigma) at a concentration of 1000ng/kg/min for 28 days (see Supplement I for more details on the infusion model). Mice were then allowed to recover for 28 days, at which time the suprarenal aortas were harvested and tested mechanically again following previous procedures.

Mechanical Testing. Briefly, the aortas were tested using cyclic pressure-diameter and axial force-length protocols performed in a temperature-controlled Hanks Balanced Salt Solution containing calcium (HBSS, Invitrogen). Specifically, vessels were cyclically pressurized from 10-140 mmHg at the *in vivo* axial stretch and at stretches 5% above and below the *in vivo* value. The vessels were then cyclically loaded from 0-2.5 g while maintained at constant pressures of 60, 100, and 140 mmHg.

Histology. After mechanical testing, vessels were placed in paraformaldehyde at their unloaded state for at least one hour and immersed in a cryoprotectant (30% sucrose) overnight. Vessels were frozen in optimum cutting temperature compound cooled with liquid nitrogen and stored in a -80°C freezer. Frozen samples were sectioned at 5 microns and stained with Verhoeff-Van Gieson (VVG) to identify elastin, PicroSirius Red to identify fibrillar collagen, Oil Red O to identify lipids, Alician Blue to identify glycosaminoglycans, and von Kossa to identify calcium deposits. Vessels were also stained for CD68 to look at macrophages and alpha-Smooth Muscle Actin antibody stain to identify functional smooth muscle cells.

Results

Pressure-diameter and force-length biaxial data reveal the characteristic behavior of the native (i.e. undisturbed) suprarenal aorta of the ApoE -/- mice (Figure 5.1). For increased clarity in presentation, a reduced number of data points (symbols) are shown in the figure. Also shown are the theoretical fits to the data (solid curves) as determined using Equation 5.3. The best-fit parameter values for all vessels are listed in Table 5.1.

Angiotensin-II infusion resulted in dissecting aneurysms in the suprarenal aorta in 6 of the 25 ApoE -/- mice studied (Table 5.1), with the mean unloaded maximum diameter of the 6 lesions being 2.25 ± 0.20 mm. Thus, the success rate, defined by generating an aneurysmal dilation (defined as an increase in maximum diameter of 1.5 fold or greater) was 24%, while 60% of our mice showed no dilations present throughout the aorta. Table 5.2 lists the pertinent information for animals with aneurysmal dilations. Table 5.3 gives the starting and ending weights for each group of mice. The initial weight of mice that developed aneurysmal dilations by the end of the 4 weeks averaged 26.1 g, which was significantly higher ($p>0.05$) than the mice that did not develop any dilations (24.2 g). The ending weights of the three groups were not statistically different.

Pressure-diameter and force-length data revealed a characteristically nonlinear behavior similarly of the normal aorta, but with significantly diminished distensibility and extensibility (~45% decrease in distensibility and ~83% decrease in *in vivo* axial stretch) (Figure 5.2). For purposes of increased clarity in presentation, a reduced number of data points are shown in the figure. Pressure-diameter and pressure-force

plots for all vessels can be found in Supplement III (Figure 5.7-5.11). The most apparent difference between these data and those for native suprarenal aortas (Figure 5.1) is the lack of a sigmoidal shape pressure diameter response. Loss of a sigmoidal shape is suggestive of a lowered elastin-to-collagen ratio, as would be expected in an aneurysmal aorta. There is a moderate increase in force as well in the dilated vessel at *in vivo* stretch.

Table 5.1. Angiotensin-II Infusion results.

	Aneurysmal Dilation	**Sub-Aneurysmal Dilation**	**Died**	**No Dilation**
Ang-II Infused (n=25)	24%	4%	12%	60%

Table 5.2. Mean values of relevant data on age, weight, and geometry of the dilated suprarenal aorta. Note that the length and outer diameter are given in the unloaded configuration.

Vessel	**Age (wks)**	**Weight (g)**	**lambda (--)**	**l_o** (mm)	**OD_o (um)**
Ang-II	12.3 ± 0.5	28.8 ± 5.5	1.13 ± 0.08	6.90 ± 0.56	2250 ± 198

Table 5.3. Initial and ending weights for the 3 major groups of mice.

	Initial Weight (g)	**Ending Weight (g)**
Aneurysmal Dilation	26.1 ± 2.1	28.8 ± 5.5
Sub-Aneurysmal Dilation	23.3	30.2
No Dilation	24.2 ± 1.8	28.8 ± 1.5

Figure 5.3 shows cross-sectional images of an unstained, dilated suprarenal aorta from the proximal to distal ends. One can see that in the region of the diaphragm (a), the aorta appears normal, but as we move distally along the aorta, there is a large region of plaque (b). From there, the plaque is replaced by a region defined by a false lumen (c-e), which again becomes a plaque region at the shoulder region of the dilation (f). The final panel (g) is that of the aorta between the two renal arteries; the aorta has regained its normal appearance.

Histological results can be seen in Figure 5.4. One can see the fully intact elastic lamina in the medial portion of the aorta (a), the presence of smooth muscle actin in the media (indicating normally functioning SMC) and in the hyperproliferative mass in the adventitial region (likely myofibroblasts that have migrated into the vessel wall) (b), and the presence of glycosaminoglycans (GAGs) in the media and the mass (c).

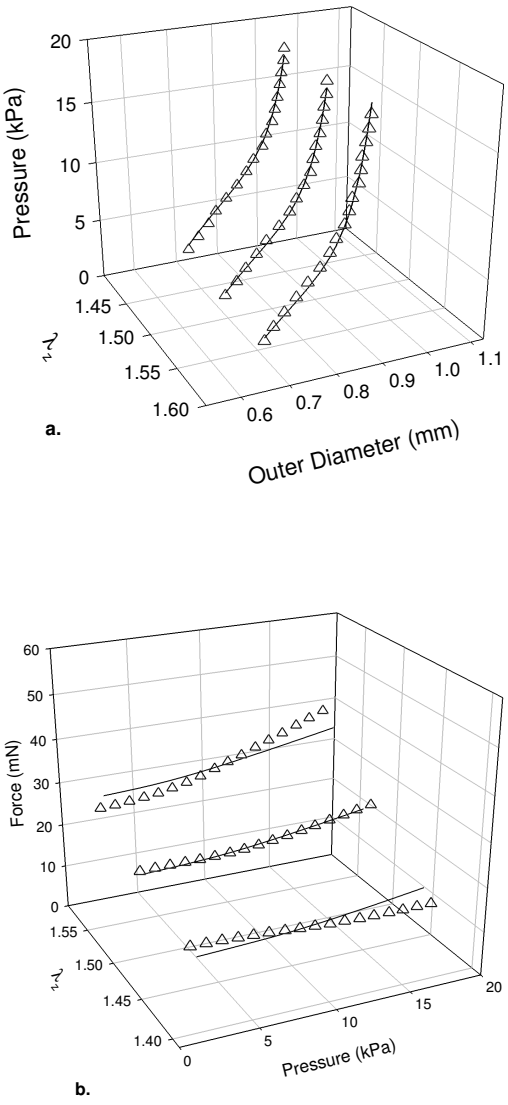

Figure 5.1. Representative pressure-diameter (a) and force-length (b) data (symbols) for the native ApoE-/- suprarenal aorta. The solid lines are the fits from equation 5.3.

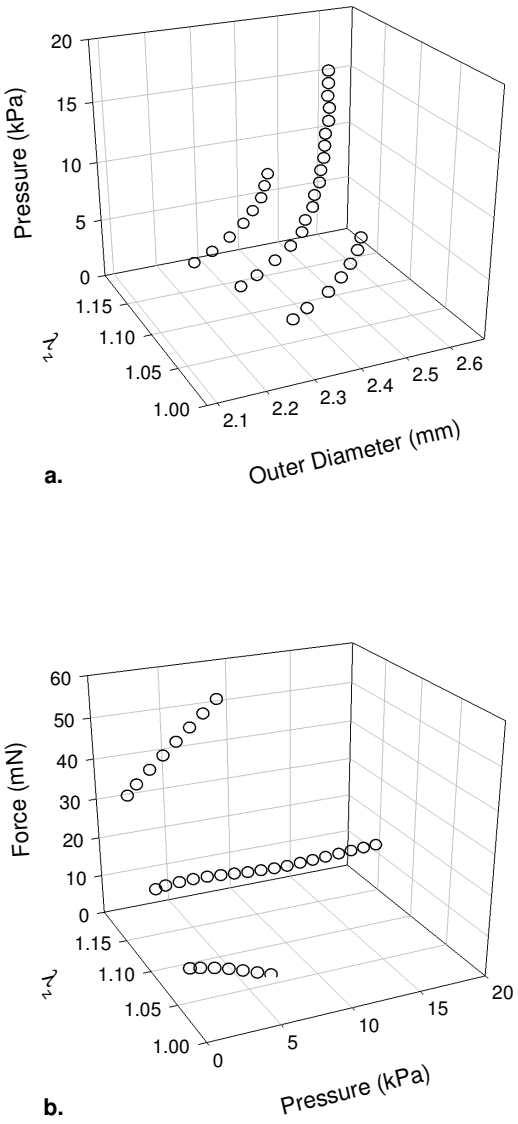

Figure 5.2. Representative (a) pressure-diameter and (b) axial force-length behavior for an ApoE-/- Ang-II infused and dilated suprarenal aorta.

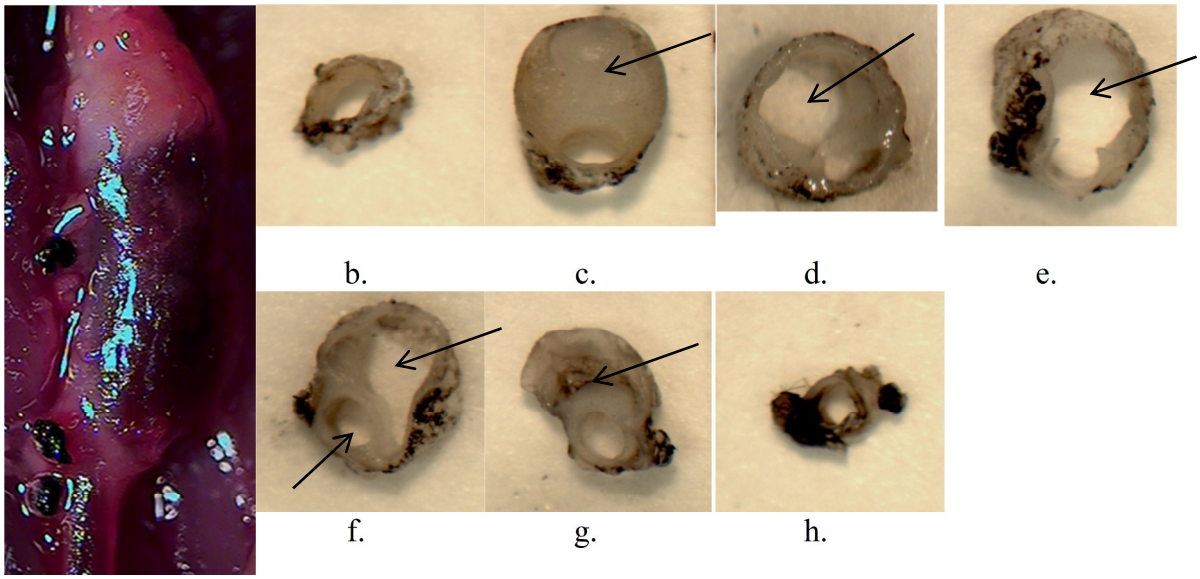

Figure 5.3. (a) *In vivo* image of a dissecting aneursym in the suprarenal aorta. (b-h) Cross-sections of a dilated suprarenal aorta from the proximal end (b) to the distal end (h). Sections (b) and (h) appear to be a relatively normal suprarenal cross-sections. (c) is the proximal shoulder region of the dilation and has what appears to be a large atherosclerotic plaque (arrow). (d-f) The plaque is no longer present and in its place is a false lumen, the arrow indicates the false lumen location. (g) The false lumen is no longer present and it appears that again there is a plaque in this shoulder region of the dilation/dissection.

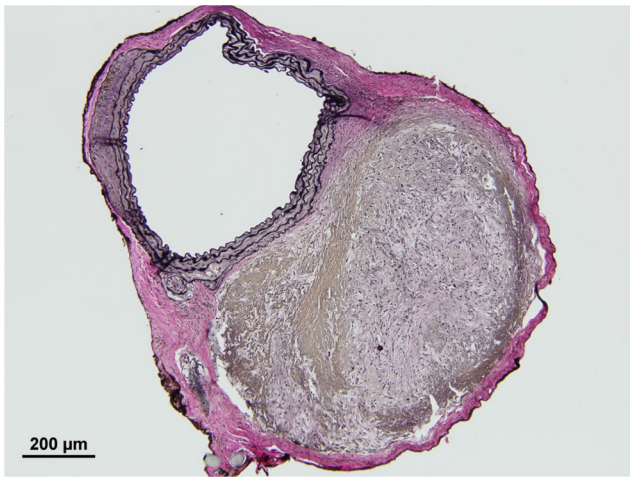

a

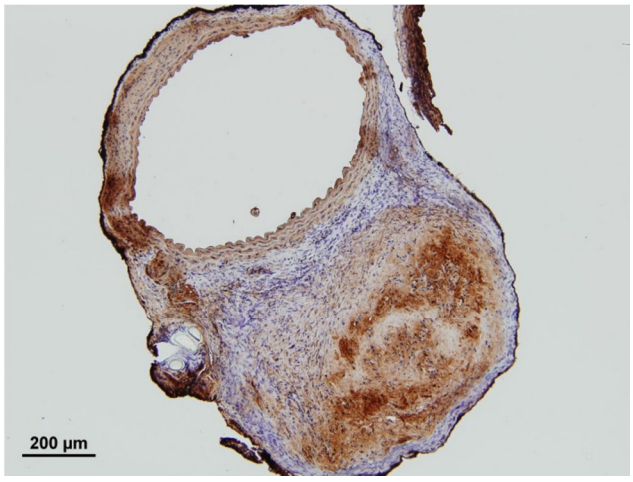

b

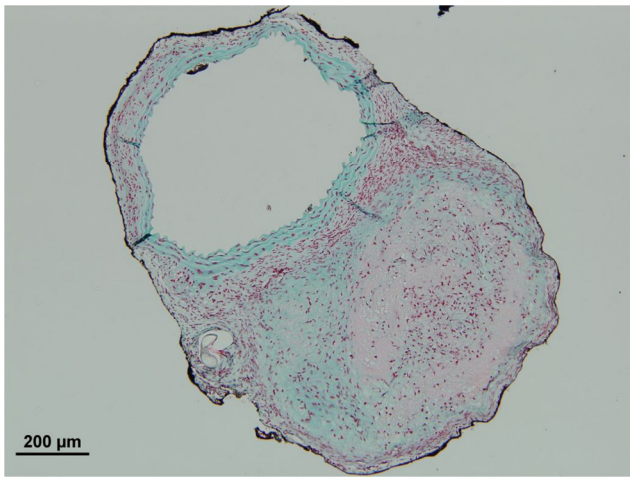

c

Figure 5.4. Histological images of the dilated region of the suprarenal aorta. (a) VVG staining, elastin is stained black, (b) smooth muscle actin staining, actin is stained brown, (c) Alcian Blue staining, GAGs stained blue.

Discussion

An aneurysm is generally defined to be a localized dilation (greater than 50%) in which the vessel wall thins weakens. Instead of the widely reported aneurysm formation with this model, consistent with Saraff et al. (2003), we found Ang-II mediated dissecting aneurysms rather than true aneurysms. In other words, rather than a wall thinning and dilation occurring as is typical of an AAA, we found the wall thickness increased and a false lumen formed. We found that Ang-II induces an atherosclerotic plaque initiated dissection to occur. It appears that the presence of an atherosclerotic plaque is necessary for a dissection and dilation to occur in the suprarenal aorta of the ApoE -/- mice. This apparent necessity is in contrast to other groups reporting AAA formation in C57 wild-type mice (Deng et al., 2003).

Mice in the 8-12 week age range that are fed a normal diet do not have many plaques in the aorta, which resulted in a lower dissection rate than has been reported in older mice using the same method. Using mice as young as 6 months, groups have reported a success rate of 80% or greater (Choke et al. 2010; Deng et al. 2003; Zhang et al. 2009). The lower percentage of lesion development in this study may be explained by our use of younger mice. The aortas of older mice would be expected to be stiffer, and thus expected to behave, mechanically, different than aortas of younger mice. As such, the effects of Ang-II might be expected to be lessened in younger mice.

As Table 5.1 indicates, twelve percent of our mice died. Unlike the deaths reported by Choke (2010) and others that were primarily ruptured AAAs, these deaths were due solely thoracic bleeds. The aortic arch ruptured in these mice between days 7

and 17 of infusion. Cao et al. (2010) reported a nearly equal prevalence of rupture in the AAA as in the arch region; however, in mice of the same age, we experienced only ruptures in the arch region. We found no evidence of non-fatal bleeding in the abdominal cavity as did Cao and colleagues.

In the suprarenal aortas that did dissect and dilate, at least the proximal portion of the dissection and dilation contained a plaque. In some cases the entire suprarenal aorta appeared to have a plaque. One suprarenal vessel had a dilation that could not be defined as aneurysmal in size (>50% increase in outer diameter) at the end of 28 days. This pressure-diameter curve of this dilation lies between the native and grossly dilated vessels (Figure 5.5). The mice that did not form dilations in the suprarenal nor die from thoracic aorta rupture rarely had any evidence of atherosclerosis in any portion of the aorta.

In Figure 5.6, the acute effects of elastase on the infrarenal aorta are compared to the dissecting aneurysm that results from chronic exposure to Ang-II in the suprarenal aorta. We can see here two striking differences between the two vessels. The first is the difference in diameters. Although these are 2 different vessels, with different initial unloaded diameters, the increase in outer diameter of the elastase-treated vessel was sub-aneurysmal at ~41% increase in loaded outer diameter. The second difference between these two vessels is the higher distensibility (due to collagen turnover) of the Ang-II infused vessel at lower pressures. Dilation is still possible in the dissected suprarenal, whereas, in the elastase-treated vessel the collagen is maximally stretched (due to an acute loss of elastin), preventing any dilation from occurring. Both models induce a

stiffening of their respective vessels, such that after some point of pressurization, dilation is no longer possible. Both vessels have a decreased range for dilation.

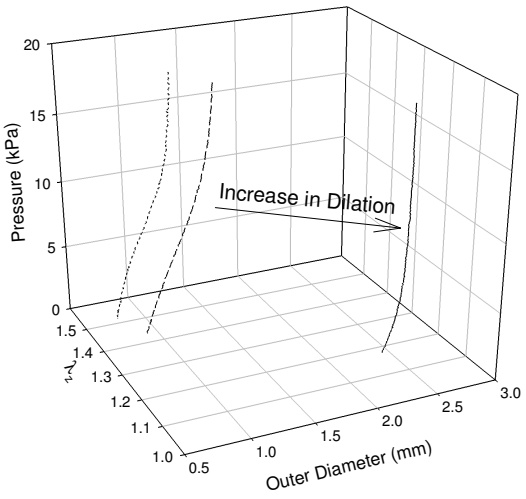

Figure 5.5. Pressure Diameter curves for control, mildly-dilated, and aneurysmally dilated suprarenal aortas due to the chronic infusion of Ang-II.

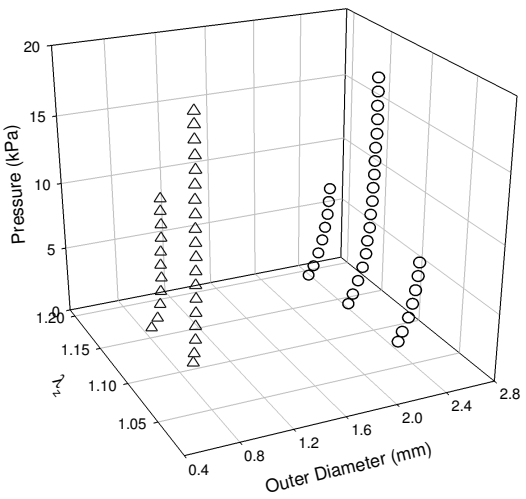

Figure 5.6. Representative plot of the pressure-diameter of an infrarenal aorta after exposure to porcine pancreatic elastase (triangles) and a suprarenal aorta after Ang-II infusion developed a dissecting aneurysm.

Despite the characteristic wall stiffening and increase in diameter, histology shows that the Ang-II infusion model is a poor model of AAA. One would have expected to see elastin fragmentation, smooth muscle cell apoptosis, and wall thinning in a true aneurysm model. While this is not a good model for AAA, histology and previous work (Saraff et al., 2003) may indicate that this could be a nice model for aortic dissection, about which little is understood. This reminds us of the necessity of being careful when creating animal models for human conditions, this aortas in this model do exhibit some of the characteristic properties expected in AAA, but upon closer examination do not exhibit the characteristics required to be defined as AAA lesions.

Supplement I

Various techniques exist for Ang-II infusion; however, we learned that some methods work better than others. We found that we were most successful using the following steps:

1) Remove Ang-II from the glass container it is sold in, despite information from Sigma, even at high concentrations, significant amounts of Ang-II are lost when dissolved into solution.
2) Use sterile normal saline. Some groups recommend using acetic acid to "stabilize" the Ang-II, but this is unnecessary as Ang-II is stable in solution. Preparing with acetic acid will create dilatations, however this is likely due more to the effects of the acetic acid and not the Ang-II, as acetic acid denatures collagen.
3) Prime in no more than 500mL sterile saline regulator side facing up. Use just enough saline to surround and cover the pump, use of too much and Ang-II will begin to leach out due to osmosis.
4) Prime for 24 hours at 37 degrees. Priming for longer results in Ang-II being released. Alcet recommends a 48 hour priming, so it is necessary to add one day to the presumed time of Ang-II exposure.
5) The use of injected anesthetic requires a very precise weight-based dosing, as in correct dosage will result in the death of the animal. Use of isoflurane is preferred.

6) Pump insertion can be done from lower on the back, just be sure to implant the pump regulator side first.
7) The insertion incision can be closed with wound glue available for veterinary use. This avoids concerns of skin tearing when using wound clips or sutures.

Supplement II

Data Analysis. To determine the native properties of the ApoE-/- suprarenal aorta, mechanical testing was performed as previously described on non-infused mice. This biaxial data were then used for constitutive modeling. The data were converted to mean circumferential and axial Cauchy stresses using standard formulas (Humphrey 2002)

$$t_{\theta\theta}^{exp} = \frac{P^{exp}a}{h}, \;\; t_{zz}^{exp} = \frac{f^{exp}}{\pi h(2a+h)} \tag{5.1}$$

where *a* is the inner radius in any loaded state and h is the associated thickness of the wall as calculated using wall volume

$$V = \pi(B-A)l \;\; , \;\; a = \sqrt{b^2 - \bar{V}/(\pi l)} \tag{5.2}$$

The applied axial force on the artery is given by $f^{exp} = f_T^{exp} + \pi a^2 P^{exp}$, where f_T^{exp} is measured by the force transducer and P^{exp} is measured by the pressure transducer.

Briefly, a 2D model "four-fiber family" hyperelastic constitutive model (Ferruzzi et al., 2011) was used, assuming that the radial component is negligible. This model has proven useful in capturing biaxial mechanical responses of diverse mouse arteries (Eberth et al., 2009b; Gleason et al., 2008; Wan et al., 2010) A strain-energy function of the following format was employed:

$$W = \frac{c}{2}(I_c - 3) + \sum_{k=1-4} \frac{c_1^k}{4c_2^k}\{exp[c_2^k((\lambda^k)^2 - 1)^2] - 1\} \quad (5.3)$$

$$I_c = \lambda_r^2 + \lambda_\theta^2 + \lambda_z^2 \quad (5.4)$$

$$\lambda^k = \sqrt{\lambda_\theta^2 sin^2\alpha^k + \lambda_z^2 cos^2\alpha^k} \quad (5.5)$$

$$\{\alpha^1 = 0, \alpha^3 = -\alpha^2, \alpha^4 = \pi/2\} \quad (5.6)$$

where α^k is the angle of the k^{th} fiber family with respect to the axial direction and the constants c, c_1^k, and c_2^k are material parameters found via nonlinear regression.

Best-fit values of the unknown parameters in equation (A-3) were determined using a nonlinear least squares minimization of the error *e* between the theoretically predicted (*theory*) and experimentally inferred (*exp*) applied loads, namely

$$e = \sum_1^N \left[\left(\frac{P^{theory} - P^{exp}}{P^{avg}}\right)^2 + \left(\frac{F^{theory} - F^{exp}}{F^{avg}}\right)^2\right]_i \quad (5.7)$$

where *N* is the total number of data points (i.e., equilibrium configurations) for all experimental protocols combined for each specimen and *avg* denotes the overall average value. The error *e* was minimized using the built-in function *lsqnonlin* in MATLAB, subject to physical constraints that $c, c_1^i c_2^i \geq 0$ and $0 \leq \alpha_o \leq \pi/2$ due to the symmetry of the diagonal fibers.

Table 5.4. Best-fit model parameters (equation 5.3).

		Axial		Circumferential		Diagonal		
Vessel	**c (kPa)**	**c_1 (kPa)**	**c_2**	**c_1 (kPa)**	**c_2**	**c_1 (kPa)**	**c_2**	**Angle (deg)**
1	10.49	19.76	0.10	7.81	7.86E-10	0.49	5.17E-01	89.99
2	8.10	30.29	0.18	7.16	4.39E-14	0.44	1.98	50.82
3	6.92	27.82	3.26	8.69	1.86E-08	0.80	5.66	36.72
4	5.59	13.10	0.31	9.99	4.57E-11	0.60	2.46	52.63
5	15.64	19.20	0.11	4.45	0.09	0.60	1.63	27.10
6	14.28	14.94	0.03	8.64	0.08	0.49	1.40	37.25
Mean	10.17 ± 4.07	20.85 ± 6.88	0.67 ± 1.27	7.79 ± 1.89	0.03 ± 0.05	0.57 ± 0.13	2.27 ± 1.78	49.08 ± 22.20

Table 5.5. Animal information. Note that length, outer diameter, and thickness are given for the unloaded configuration.

Vessel	**Age (wks)**	**Weight (g)**	**l_z (--)**	**l_o** (mm)	**OD_o (um)**	**H_o (um)**	**ri (um) @80 mmHg**	**h (um) @80 mmHg**
ApoE -/-	10.5 ± 1.6	26.7 ± 2.8	1.41 ± 0.15	3.66 ± 0.63	758 ± 60	127 ± 24	465 ± 68	56 ± 12

Supplement III

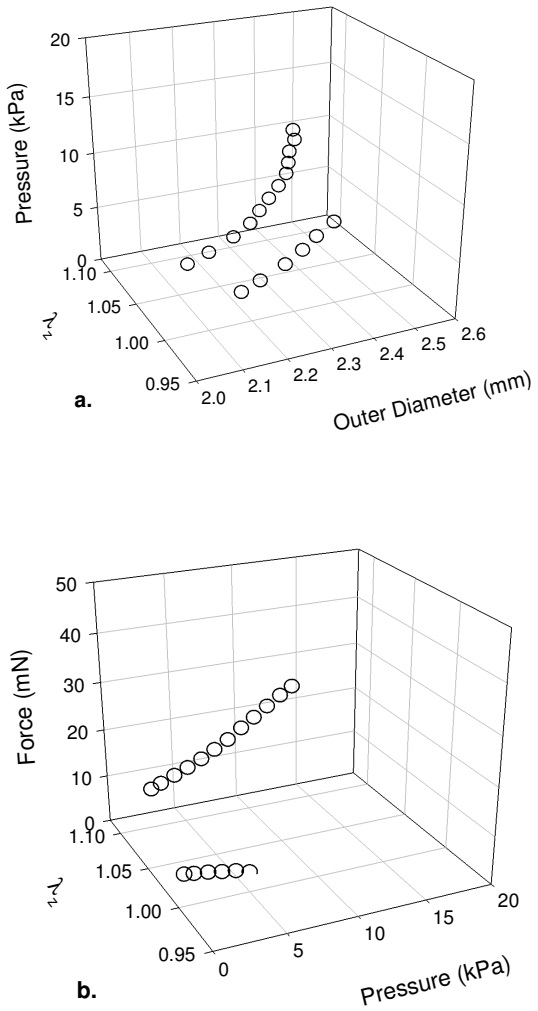

Figure 5.7. Pressure-diameter and pressure-force data for aneurysm #1.

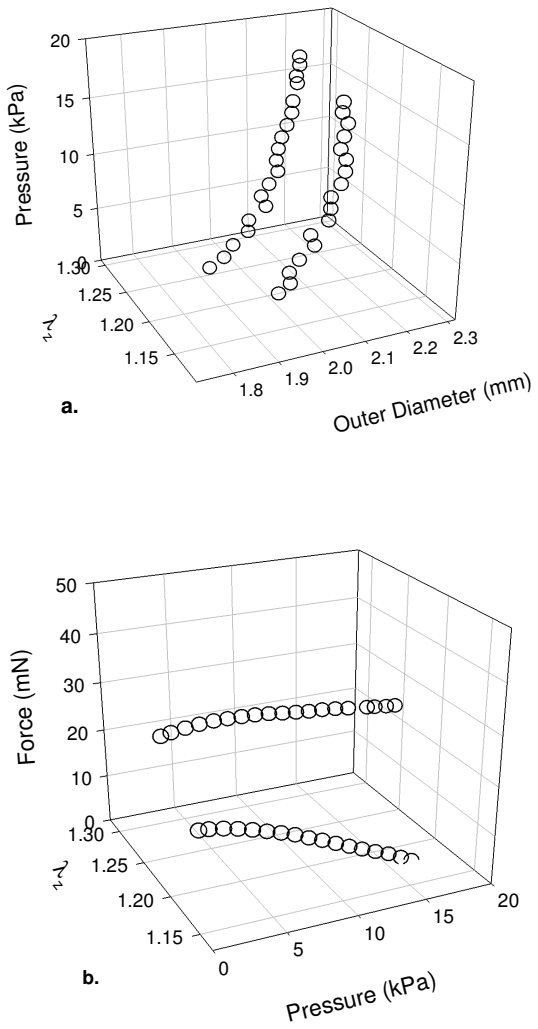

Figure 5.8. Pressure-diameter and pressure-force data for aneurysm #2.

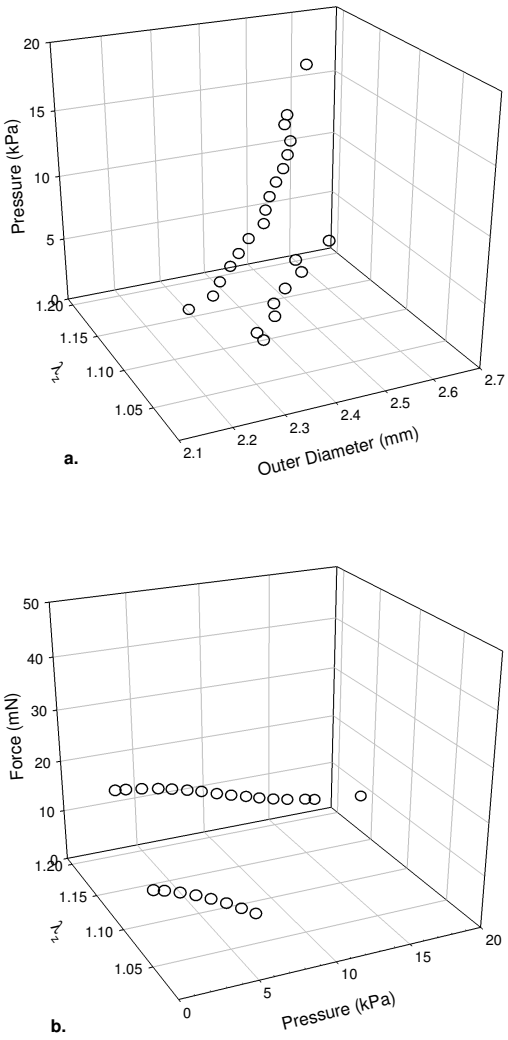

Figure 5.9. Pressure-diameter and pressure-force data for aneurysm #3.

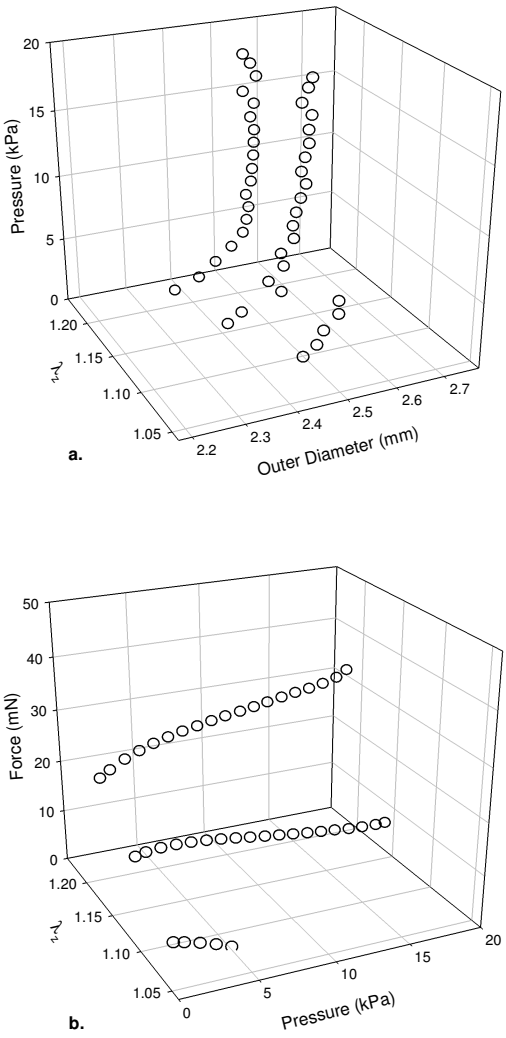

Figure 5.10. Pressure-diameter and pressure-force data for aneurysm #4.

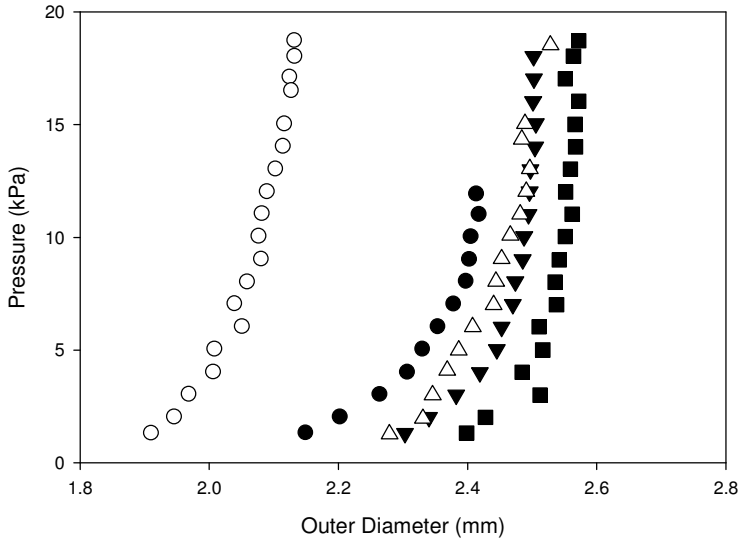

Figure 5.11. Pressure-diameter plots at the *in vivo* axial stretch of each of the 5 ApoE-/- Ang-II infused dilated suprarenal aortas.

CHAPTER VI

SUMMARY AND FUTURE DIRECTION

Understanding the mechanical properties of Abdominal Aortic Aneurysms (AAAs) is paramount to improving treatment of this deadly condition. As a step towards this understanding, we have made strides in understanding not only the mechanical behavior and constitutive parameters of the two vessels that experience AAA in different mouse models, but also the effects of the three major components of AAA formation: elastin degradation, smooth muscle cell dysfunction, and inflammation.

We have presented a first of its kind study looking at the solid mechanics of the infrarenal and suprarenal aorta to try to understand why in non-targeted models of AAAs (like Ang-II infusion) form exclusively in the suprarenal aorta whereas in humans the lesions preferentially form in the infrarenal aorta. Previous studies have looked at the hemodynamics, but have found that the hemodynamics alone are not responsible. We found that the major difference between the two vessels is the elastin content in the suprarenal aorta. We know that hemodynamics plays an important role in atherosclerosis development, causing plaques to form preferentially in the suprarenal aorta of ApoE-/- mice. We believe that after an initiating event due to hemodynamics, that the vascular mechanics take over to form AAA lesions.

Next we examined at the mechanical and constitutive effects of an acute loss of functional elastin via intraluminal exposure to elastase. Surprisingly, although a relatively common model for AAA formation, biaxial mechanical data have not been

collected previously on this vessel. We found, not surprisingly, that the vessel is much stiffer after elastase exposure, such that when pressurized the vessel experiences minimal distension. This is due to the loss of collagen undulation caused by highly pre-stretched elastin. The constitutive parameter for the elastic component is nearly zero and the collagen fibers experience much more stress when growth and remodeling is not allowed to occur.

The loss of smooth muscle cell contractility is expected in human lesions due to the loss of smooth muscle cells. Indeed, mutations in α-SMA have also been found in patients with TAAD. Some 1-D contractility testing has been performed on the aorta in the α-SMA null mouse, but no biaxial mechanics. We looked at the wild-type (+/+), heterozygous (+/-), and null (-/-) α-SMA mice. Surprisingly, we found that the passive mechanics and constitutive parameters between the three groups to be nearly identical. The *in vivo* stretch was not statistically different, which would indicate the absence of any lengthening of the vessel as a compensatory mechanism (cf. Humphrey et al., 2009). We found that the constitutive parameter for the elastic component of the vessel to be higher in the (+/-) mice, which histology will be able to clarify for us.

Finally, we performed biaxial mechanical tests on Ang-II-infused ApoE-/- mice. This is another common model for AAA formation, and again surprisingly the mechanics of the vessel have rarely been discussed. This model is a poor model of AAA, instead of a wall dilating and thinning as seen in AAAs, this model results in a dissecting aneurysm, not only with a false lumen, but with no smooth muscle cell apoptosis, no elastin fragmentation, and adventitial growth marked myofibroblast

infiltration into the wall. Results are similar to what one might find in a wound healing response. We found that in these young mice, atherosclerotic plaques were often an initiating point for dissections to occur. Although the pressure-diameter curves show a similar stiffness to the elastase vessel, more dilatation occurs in these vessels as the collagen has likely regained some of its undulation during collagen turnover in evolving configurations. The pressure-force behavior of these vessels is similar to a native vessel, as opposed to the pressure-force behavior of the elastase vessels.

Improved devices and methods are necessary in order to estimate constitutive parameters from the Ang-II-infusion model for dissecting aneurysms. The mathematical model used in this work makes the assumptions that the vessel is a thin-walled, axisymmetric cylinder. With a dissecting aneurysm, this is not true. A new device has been developed and is beginning to be tested on small arteries, but this is beyond the scope of the present work. This novel device employs the use of stereo-digital image correlation to quantify size, shape, and deformation of an artery, in order to look at full-surface strains. This does not result in constitutive parameters, but does allow for full-field strain information to be gathered on small vessels.

Improvements can be made, and should be made to the constitutive equation used herein. The current constitutive equation works well for a basic tube geometry, but does not capture the coupling of microstructure components, like elastin and collagen. The ability to capture this coupling will allow us to better describe the behavior of a vessel under a variety of conditions (like elastase exposure). With the complicated geometry of

dissections and AAAs, more complicated models necessarily mean finite element models.

Longitudinal information needs further exploration. How the mechanics of the aorta change as an aneurysm develops is a current void in the literature. There is also a pressing need to understand the natural history of the AAA and how the mechanics correlate to the cellular processes involved. A study which involved 4-5 time points during the 28 day AAA development period could provide information on the effects of the different stages. Longitudinal studies could be completed in conjunction with MRI studies. With MR studies, the first point of interest would be in determining the validity of the observation that the plaque appears to be the initiating factor in the dissection and dilation. MR studies would allow us to monitor the natural history of the lesion as the geometry changes.

Our goal was to understand the mechanics of the individual components of aneurysm formation. The inflammation model and the α-smooth muscle actin null mice elicited unexpected results. We used the Ang-II model based on results that others have published, but we need to do better. By using mice models, we can look at individual components of AAA development as well as the time courses of development. This type of work allows us to develop hypotheses directing what should be measured or examined in human subjects.

REFERENCES

Ailawadi,G., Moehle, C.W., Pei, H., Walton, S.P., Yang, Z., Kron, I.L., Lau, C.L., Owens, G.K., 2009. Smooth muscle phenotypic modulation is an early event in aortic aneurysms. Journal of Thoracic and Cardiovascular Surgery 138, 1392-1399.

Amirbekian, S., Long, R.C., Consolini, M.A., Suo, J., Willett, N.J., Fielden, S.W., Giddens, D.P., Taylor, W.R., Oshinski, J.N., 2009. *In vivo* assessment of blood flow patterns in abdominal aorta of mice with MRI: implications for AAA localization. American Journal of Physiology 297, H1290-1295.

Anidjar, S., Salzmann, J.L., Gentric, D., Lagneau, P., Camilleri, J.P., Michel, J.B., 1990. Elastase-induced experimental aneurysms in rats. Circulation. 82, 973-981.

Anidjar, S., Dobrin, P.B., Chejfec, G., Michel, J.B., 1994. Experimental study of determinents of aneurysmal expansion of the abdominal aorta. Annals of Vascular Surgery. 8, 127-136.

Baek, S., Rajagopal, K.R., Humprhey, J.D., 2006. A theoretical model of enlarging intracranial fusiform aneurysms. Journal of Biomechanical Engineering 128, 142-149.

Baek, S., Gleason R.L., Rajagopal, K.R., Humphrey, J.D., 2007. Theory of small on large: potential utility in computations of fluid-solid interaction in arteries. Computer Methods in Applied Mechanics and Engineering 196, 3070-3078.

Bunce, D.F.M., 1974. Atlas of Arterial Histology. Warren H. Green, Inc. St. Louis, MO.

Cao, R.Y., St. Amand, T., Ford, M.D., Piomelli, U., Funk, C.D., 2010. The murine angiotensin II-induced abdominal aortic aneurysm model: rupture risk and inflammatory progression patterns. Frontiers in Pharmacology 1, 1-9.

Cassis, L.A., Gupta, M., Thayer, S., Zhang, Z., Charnigo, R., Howatt, D.A., Rateri, D.L., Daugherty, A., 2009. Ang II infusion promotes abdominal aortic aneurysms independent of increased blood pressure in hypercholesterolemic mice. American Journal of Pathology 296, H1660-1665.

Cheng, Z.J., Vapaatalo, H., Mervaala, E., 2005. Angiotensin II and vascular inflammation. Medical Science Monitor 11, RA194-205.

Choke, E., Cockerill, G.W., Dawson, J., Howe, F., Wilson, W.R., Loftus, I.M., Thompson, M.M., 2010. Vascular endothelial growth factor enhances angiotensin-ii induced aneurysm formation in apolipoprotein E-deficient mice. Journal of Vascular Surgery 52, 159-166.

Daughtery, A., Cassis, L.A., 2004. Mouse models of abdominal aortic aneurysms. Arteriosclerosis, Thrombosis, and Vascular Biology 24, 429-434.

Deguchi, J.O., Huang, H., Libby, P., Aikawa, E., Whittaker, P., Sylvan, J., Lee, R.T., Aikawa, M., 2009. Genetically engineered resistance for MMP collagenases promotes abdominal aortic aneurysm formation in mice infused with angiotensin-II. Laboratory Investigation 89, 315-326.

Deng, G.G., Martin-McNulty, B., Sukovich, D.A., Freay, A., Halks-Miller, M., Thinnes, T., Loskutoff, D.J., Carmeliet, P., Dole, W.P., Wang, Y.X., 2003. Urokinase-type plasminogen activator plays a critical role in angiotensin II-induced abdominal aortic aneurysm. Circulation Research 92, 510-517.

Dobrin, P.B., Canfield, T.R., 1984. Elastase, collagenase, and the biaxial elastic properties of dog carotid artery. American Journal of Physiology. 247, H124-131.

Dobrin, P.B., Grey, W.C., 1985. Elastase, collagenase and the radial elastic properties of arteries. Experimentia 41, 1040-1042.

Duo, M.M., Dalman, R.L., 2010 Hemodynamic influences on abdominal aortic aneurysm disease: application of biomechanics to aneurysm pathophysiology. Vascular Pharmacology 53, 11-21.

Dye, W.W., Gleason, R.L., Wilson, E., Humphrey J.D., 2007. Biaxial biomechanical behavior of carotid arteries in two knockout models of muscular dystrophy. Journal of Applied Physiology 103, 664-672.

Eberth, J.F., Gresham, V.C., Reddy, A.K., Popovic, N. Wilson, E., Humphrey, J.D., 2009a. Importance of pulsatility in hypertensive carotid artery growth and remodeling. Journal of Hypertension 27, 2010-2021.

Eberth, J.F., Taucer, A.I., Wilson, E., Humphrey, J.D., 2009a. Mechanics of carotid arteries from a mouse model of Marfan Syndrome. Annals of Biomedical Engineering 37, 1093-1104.

Ferruzzi, J., Collins, M.J., Yeh, A.T., Humphrey, J.D., 2011. Mechanical

assessment of elastin integrit in fibrillin-1 deficient carotid artieres: implications for Marfan syndrome. Cardiovascular Research (in press).

Ferruzzi, J., Vorp, D.A., Humphrey, J.D., 2011. A structurally-motivated constitutive relation for the biaxial mechanical behavior of human aorta and abdominal aortic aneurysms. Journal of the Royal Society Interface 8, 435-450.

Fonck, E., Prod'hom, G., Roy, S., Augsburger, L., Rüfenacht, D.A., Stergiopulos, N., 2007. Effect of elastin degradation on carotid wall mechanics as assessed by a constituent-based biomechanical model. American Journal of Physiology: Heart and Circulatory Physiology 292, H2754-H2763.

Gleason, R.L., Grey, S., Wilson, E., Humphrey, J.D., 2004. A multiaxial computer-controlled organ culture and biomechanical device for mouse carotid arteries. ASME Journal of Biomechanical Engineering 126, 787-795.

Gleason, R.L., Humphrey, J.D., 2005. A 2D constrained mixture model for arterial adaptations to large changes in flow, pressure, and axial stretch. Mathematical Medicine and Biology 22, 347-369.

Gleason, R.L., Dye, W.W., Wilson, E., Humphrey, J.D., 2008. Quantification of the mechanical behavior of carotid arteries from wild-type, dystrophin-deficient, and sarcoglycan-delta knockout mice. Journal of Biomechanics 41, 3213-3218.

Goergen, C.J., Barr, K.N., Huynh, D.T., Eastham-Anderson, J.R., Choi, G., Hedehus, M., Dalman, R.L., Connolly, A.J., Taylor, C.A., Tsao, P.S., Greve, J.M., 2010. *In vivo* quantification of murine aortic cyclic strain, motion, and curvature: Implications for abdominal aortic aneurysms. Journal of Magnetic Resonance Imaging 32, 847-858.

Goergen, C.J., Azuma, J., Barr, K.N., Magdefessel, L., Kallop, D.Y., Gogineni, A., Grewall, A., Weimer, R.M., Connolly, A.J., Dalman, R.L., Taylor, C.A., Tsao, P.S., Greve. J.M., 2011. Influences of aortic motion and curvature on vessel expansion in murine experimental aneurysms. Arteriosclerosis, Thrombosis, and Vascular Biology 31, 270-279.

Guo, D.C., Pannu, H., Tran-Fadulu, V., Papke, C.L., Yu, R.K., Avidan, N., Bourgeois, S., Estrera, A.L., Safi, H.J., Sparks, E., Amor, D., Ades, L., McConnell, V., Willoughby, C.E., Abuelo, D., Willing, M., Lewis, R.A., Kim, D.H., Scherer, S., Tung, P.P., Ahn, C., Buja, L.M., Raman, C.S., Shete, S.S., Milewicz, D.M., 2007. Mutations in smooth muscle α-actin (ACTA2) lead to thoracic aortic aneurysms and dissections. Nature Genetics 39, 1488-1493.

Guo, D.C., Papke, C.L., Tran-Fadulu, V., Regalado, E.S., Vaidan, N., Johnson, R.J.

Kim, D.H., Pannu, H., Willing, M.C., Sparks, E., Pyreitz, R.E., Singh, M.N., Dalman, R.L., Grotta, J.C., Marian, A.J., Boerwinkle, E.A., Frazier, L.Q., LeMaire, S.A., Coselli, J.S., Estrera, A.L., Safi, H.J., Shete, S.S., Scherer, S.E., Raman, C.S., Buja, L.M., Milewicz, D.M., 2009. Mutation in smooth muscle alpha-actin (ACTA2) cause coronary artery disease, stroke, and moyamoya disease, along with thoracic aortic disease. The American Society of Human Genetics 84, 617-627.

Guo, X., Kassab, G.S., 2003. Variation of mechanical properties along the length of the aorta in C57bl/6 mice. American Journal of Physiolgoy 285, H2614-2622.

Hayenga, H.N., Trache, A., Trzeciakowski, J., Humphrey, J.D., 2011. Regional atherosclerotic plaque properties in ApoE-/- mice measured by atomic force, 89mmunofluorescence, and light microscopy. Journal of Vascular Research (in press).

Holzapfel, G.A., Gasser, T.C., Ogden, R.W., 2000. A new constitutive framework for arterial wall mechanics and a comparative study of material models. Journal of Elasticity 61, 1–48.

Holzapfel, G.A., Gasser, T.C., Ogden, R.W., 2004. Comparison of a multi-layer structural model for arterial walls with a fung-type model, and issues of material stability. Journal of Biomechanical Engineering 126, 264-275.

Humphrey, J.D., 2002. Cardiovascular Solid Mechanics: Cells, Tissues, and Organs. Springer-Verlag, New York.

Humphrey, J.D., Rajagopal, K.R., 2003. A Constrained mixture model for arterial adaptations to a sustained step change in blood flow. Biomechanics and Modeling in Mechanobiology 2, 109-126.

Humphrey, J.D., 2008. Vascular adaptation and mechanical homeostasis at tissue, cellular, and sub-cellular levels. Cell Biochemistry and Biophysics 50, 53-78.

Humphrey, J.D., Taylor, C.A., 2008. Intracranial and abdominal aortic aneurysms: similarities, differences, and need for a new class of computational models. Annual Review of Biomedical Engineering 10, 221-246.

Humphrey, J.D., Eberth, J.F., Dye, W.W., Gleason, R.L., 2009. Fundamental role of axial stress in compensatory adaptations by arteries. Journal of Biomechanics 42, 1-8.

Klabunde, R.E., 2005. Cardiovascular Physiology Concepts. Lippincott Williams & Wilkins, New York.

Manning, M.W., Cassis, L.A., Daugherty, A., 2003. Differential effects of doxycycline, a broad-spectrum matrix metalloproteinase inhibitor, on angiotensin-II-induced atherosclerosis. Arteriosclerosis, Thrombosis, and Vascular Biology 23,483-488.

Milewicz, D.M.Ostergaard, J.R., Ala-Kokko, L.M., Khan, N., Grange, D.K., Mendoza-Londono, R., Bradley, T.J., Olney, A.H., Ades, L., Maher, J.F., Guo, D., Buja, L.M., Kim, D., Jyland, J.C., Regalado, E.S., 2010. Denovo ACTA2 mutation causes a novel syndrome of multisystemic smooth muscle cell dysfunction. American Journal of Medical Genetics Part A 152A, 2437-2443.

Nakashima, Y., Plump, A.S., Raines, E.W., Breslow, J.L., Ross, R., 1994. ApoE deficient mice develop lesions of all phases of atherosclerosis throughout the arterial tree. Arteriosclerosis and Thrombosis 14, 133-140.

Pannu, H., Avidan, N., Tran-Fadulu, V., Milewicz, D.M., 2006. Genetic basis of thoracic aortic aneurysms and dissections: potential relevance to abdominal aortic aneurysms. Annals of the New York Academy of Science 1085, 242-255.

Rezakhaniha, R., Fonck, E., Genoud, C., Stergiopulos, N., 2011. Role of elastin anisotropy in structural strain energy functions of arterial tissue. Biomechanics and Modeling in Mechanobiology 10, 599-611.

Saraff, K., Babamusta, F., Cassis, L.A., Daugherty, A., 2003. Aortic dissection precedes formation of aneurysms and atherosclerosis in angiotensin-II infused, apolipoprotein E-deficient mice. Arteriosclerosis, Thrombosis, and Vascular Biology 23, 1621-1626.

Schildmeyer, L.A., Braun, R., Taffet, G., Debiasi, M., Burns, A.E., Bradley, A., Schwartz, R.J., 2000. Impaired vascular contractility and blood pressure homeostasis in the smooth muscle a-actin null mouse. FASEB Journal 14, 2213-2220.

Sheth, R.A., Maricevich, M., Mahmood. U., 2010. *In vivo* optical molecular imaging of matrix metalloproteinase activity in abdominal aortic aneurysms correlates with treatment effects on growth rate. Atherosclerosis 212, 181-187.

Shimizu, K., Mitchell, R.N., Libby, P., 2006. Inflammation and cellular immune responses in abdominal aortic aneurysms. Arteriosclerosis, Thrombosis, and Vascular Biology 26, 987-994.

Thompson, R.W., Curci, J.A., Ennis, T.L., Mao, D., Pagano, M.B., Pham, C.T., 2006.

Pathophysiology of abdominal aortic aneurysms: insights from the elastase-induced model in mice with different genetic backgrounds. Annals of the New York Academy of Sciences. 1085, 59-73.

Valentine, A., Cardomone, L., Baek, S., Humphrey, J.D., 2009. Complimentary vasoactivity and matrix remodeling in arterial adaptations to altered flow and pressure. Journal of the Royal Society, Interface 6, 293-306.

Vorp, D.A., 2007. Biomechanics of abdominal aortic aneurysm. Journal of Biomechics 40, 1887-1902.

Wagenseil, J.E., Nerurkar, N.L., Knutsen, R.H., Okamoto, R.J., Li, D.Y., Mecham, R.P., 2005. Effects of elastin haploinsufficiency on the mechanical behavior of mouse arteries. American Journal of Physiology 289, H1209-1217.

Wan, W., Yanagisawa, H., Gleason, R.L., 2010. Biomechanical and microstructural properties of common carotid arteries from fibulin-5 null mice. Annals of Biomedical Engineering 38, 3605-3617.

Wicker, B.K., Hutchens, H.P., Wu, Q., Yeh, A.T., Humphrey, J.D., 2008. Normal basilar artery structure and biaxial mechanical behavior. Computer Methods in Biomechanics and Biomedical Engineering 11, 539-551.

Zhang, Y., Naggar, J.C., Welzig, C.M., Beasley, D., Moulton, K.S., Park, H.J., Galper, J.B., 2009. Simastatin inhibits angiotensin II-induced abdominal aortic aneurysm formation in apolipoprotein E-knockout mice: possible role of ERK. Arteriosclerois, Thrombosis, and Vascular Biology 29, 1764-1771.

VITA

Name: Melissa Jill Collins

Address: c/o Biomedical Engineering Department Texas A&M University, College Station, TX, 77840

Email Address: Melissa.collins@tamu.edu

Education: B.S., Biological Systems Engineering, The University of Nebraska - Lincoln, 2006
PhD., Biomedical Engineering, Texas A&M University, 2011.

Publications: **Collins M.J**., M. Bersi, E. Wilson, and J. Humphrey. 2011. Comparison of suprarenal and infrarenal aortic mechanical properties: implications for mouse models of abdominal aortic aneurysms. Medical Engineering and Physics *(In press).*

Ferruzzi J., **M. Collins**, A.T. Yeh, and J.D. Humphrey. 2011. Mechanical assessment of elastin integrity in fibrillin-1 deficient carotid arteries: implications for Marfan syndrome. Cardiovascular Research *(In press).*